EXPERIENCE WITH THE BOUNDARY-ELEMENT METHOD OF NUMERICAL MODELING TO RESOLVE COMPLEX GROUND CONTROL PROBLEMS

By George J. Karabin, P.E.,[1] and Michael A. Evanto, P.G.[2]

ABSTRACT

The Mine Safety and Health Administration, Pittsburgh Safety and Health Technology Center, Roof Control Division, is routinely involved in the evaluation of ground conditions in underground coal mines. Assessing the stability of mined areas and the compatibility of mining plans with existing conditions is essential to ensuring a safe working environment for mine workers at a given site. Since 1985, the Roof Control Division has successfully used the boundary-element method of numerical modeling to aid in the resolution of complex ground control problems. This paper presents an overview of the modeling methodology and details of techniques currently used to generate coal seam, rock mass, and gob backfill input data. A summary of coal and rock properties used in numerous successful evaluations throughout the United States is included, and a set of deterioration indices that can aid in the quantification of in-mine ground conditions and verification of model accuracy is introduced. Finally, a case study is detailed that typifies the complexity of mining situations analyzed and illustrates various techniques that can be used to evaluate prospective design alternatives.

[1]Supervisory civil engineer.
[2]Geologist.
Mine Safety and Health Administration, Pittsburgh Safety and Health Technology Center, Roof Control Division, Pittsburgh, PA.

INTRODUCTION

Effective mine design has long been recognized as an essential element in establishing safe and productive mining operations. Numerous investigators have developed techniques to analyze pillar stability and maximize mining efficiency. The work of Holland and Gaddy [1964], Obert and Duvall [1967], and Bieniawski [1984], to name a few, served as a staple for mining engineers for many years. With the advent of longwall mining, new techniques were developed by Carr and Wilson [1982], Hsuing and Peng [1985], Choi and McCain [1980], and Mark [1990] to address design considerations for that technology. Most recently, the development of the Analysis of Retreat Mining Pillar Stability (ARMPS) methodology [Mark and Chase 1997] for the evaluation of retreat mining operations added an additional tool for engineers to design and evaluate full pillaring techniques.

Each of these methods can provide a reasonable estimate of pillar strength and stability under specific conditions and relatively simple mining geometries. In practice, however, situations often arise where areas of concern contain a number of pillar configurations with varying entry and crosscut widths, spacings, and orientations. Additional factors, such as non-uniform pillar lines, remanent stumps scattered throughout irregularly shaped gobs, and multiple-seam mining, can further complicate an analysis. In such instances, application of the previously mentioned empirical and analytical methods to accurately evaluate ground stability is difficult, if not totally impossible.

A primary function of the Roof Control Division, Pittsburgh Safety and Health Technology Center, is to provide technical assistance to the Mine Safety and Health Administration (MSHA) and the mining industry in the resolution of complex roof control problems. In order to evaluate mining systems not easily treated by simplified empirical or analytical methods, boundary-element numerical modeling was initiated in 1984 and expanded in 1987 with acquisition of the BESOL system from Crouch Research, Inc., St. Paul, MN. The ability of the three-dimensional (3-D) boundary-element method to model large mine areas with complex geometries has enabled the Roof Control Division to successfully simulate conditions and identify potential solutions to ground control problems in mines throughout the United States. The technique has been applied to a variety of mining scenarios, including longwall and room-and-pillar operations using both conventional and yield pillar configurations. The influence of vertical and horizontal stress has been modeled to simulate underground conditions ranging from deteriorating roof and persistent falls to areas of squeezing ground and complete pillar failure.

In the process of developing numerical models for the various mining operations analyzed during the last 10 years, a systematic simulation methodology has evolved. Techniques to estimate the necessary coal, rock, and gob backfill properties have been established, and a deterioration index was developed to quantify in-mine roof, floor, and pillar behavior to assist in calibrating model parameters and evaluating potential mine design alternatives. This paper presents a brief description of the BESOL system, an overview of the simulation process used, and details of methods used to construct models and estimate rock mechanics parameters. A discussion of the deterioration index system and details of a case study typifying an actual mine simulation and techniques used to evaluate conditions and proposed mining options is also included.

BESOL SYSTEM DESCRIPTION

BESOL is a system of computer programs for solving rock mechanics problems based on the boundary-element displacement discontinuity method of analysis. The 3-D MS221 version (yielding and multiple-seam capability) was acquired from Crouch Research, Inc., and has been used by the Roof Control Division to evaluate complex mining systems since 1987. The BESOL system is complete with graphic pre- and postprocessors that greatly simplify model construction and output data interpretation.

Figure 1 presents a generalized BESOL boundary-element model that illustrates a tabular seam or ore body surrounded by a homogenous, isotropic, linearly elastic rock mass. Input data include elastic rock mass properties and rock strength criteria, seam properties, and backfill or artificial support characteristics. A definition of the seam plane(s), detailed geometry of the excavation, mining depth, seam height, and a complete 3-D in situ stress state of the model are also required. Output capabilities include stress, strain, and displacement calculations within user-selected areas (both on and off the seam plane), failure index (Mohr-Coulomb or Hoek-Brown roof and floor safety factors) calculations at variable locations in the rock mass, and energy release estimates in yielding areas.

BESOL was selected by the Roof Control Division because it offered a number of features considered essential in simulating complex mining situations. These include:

- 3-D capability
- Large fine-mesh grid (180 by 270 elements)
- Yielding seam option (user-defined)
- Multiple-seam capability
- Backfill and artificial support materials

Other features that made the package attractive were:

- PC-based operation
- Off-seam stress/strain capability
- Failure index calculation (Mohr-Coulomb/Hoek-Brown)
- Graphic pre- and postprocessors
- Multiform hard-copy output capability

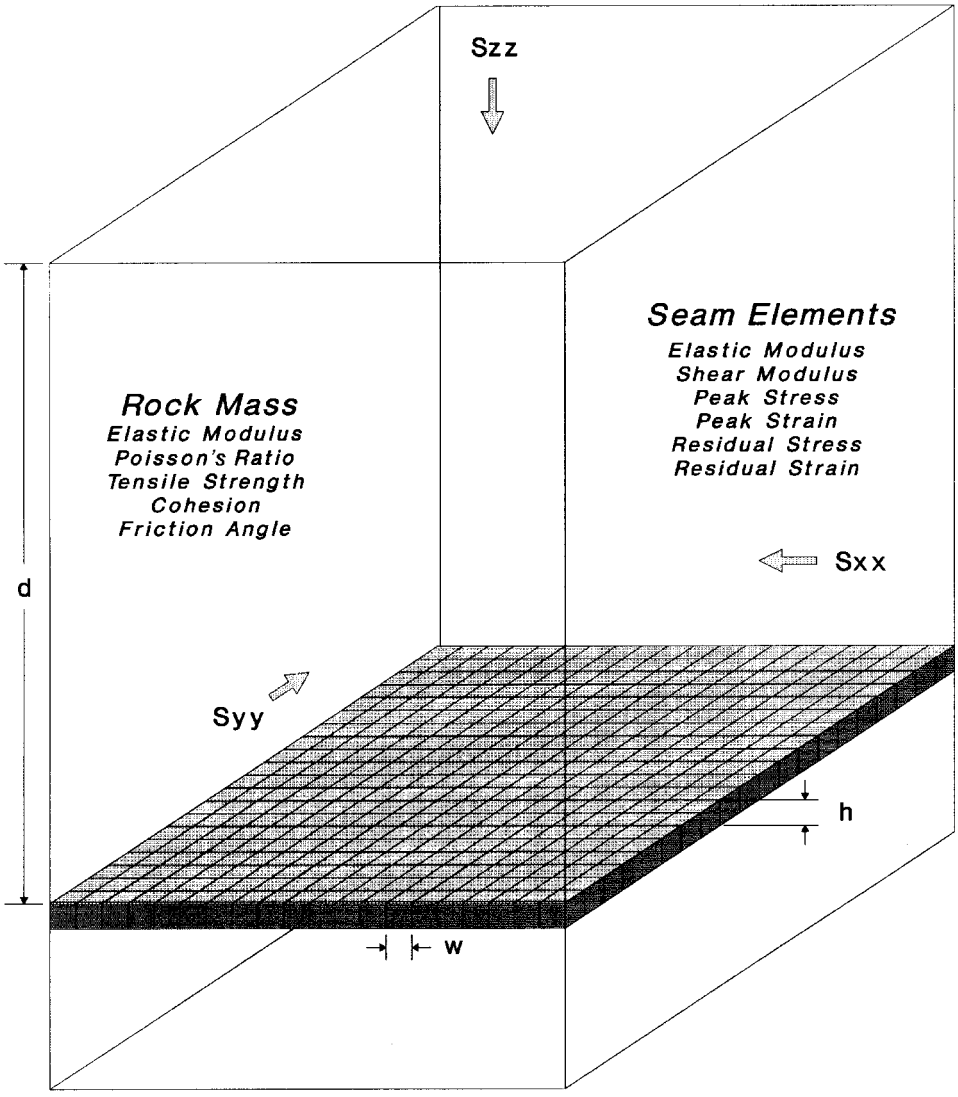

Figure 1.—Generalized BESOL boundary-element model.

SIMULATION PROCESS

Figure 2 presents an eight-step process used by the Roof Control Division during the simulation of underground mining systems. Although it is specifically directed to numerical modeling applications, it can also be used in conjunction with empirical or analytical methods.

1. *Observe Underground Areas:* This is an essential first step in solving ground control problems regardless of the methodology employed. Mine conditions should be categorized in a number of areas where differing pillar sizes, panel configurations, and overburden levels are found. The deterioration index system, which will be discussed later in this paper, can aid in the description of in-mine ground conditions.

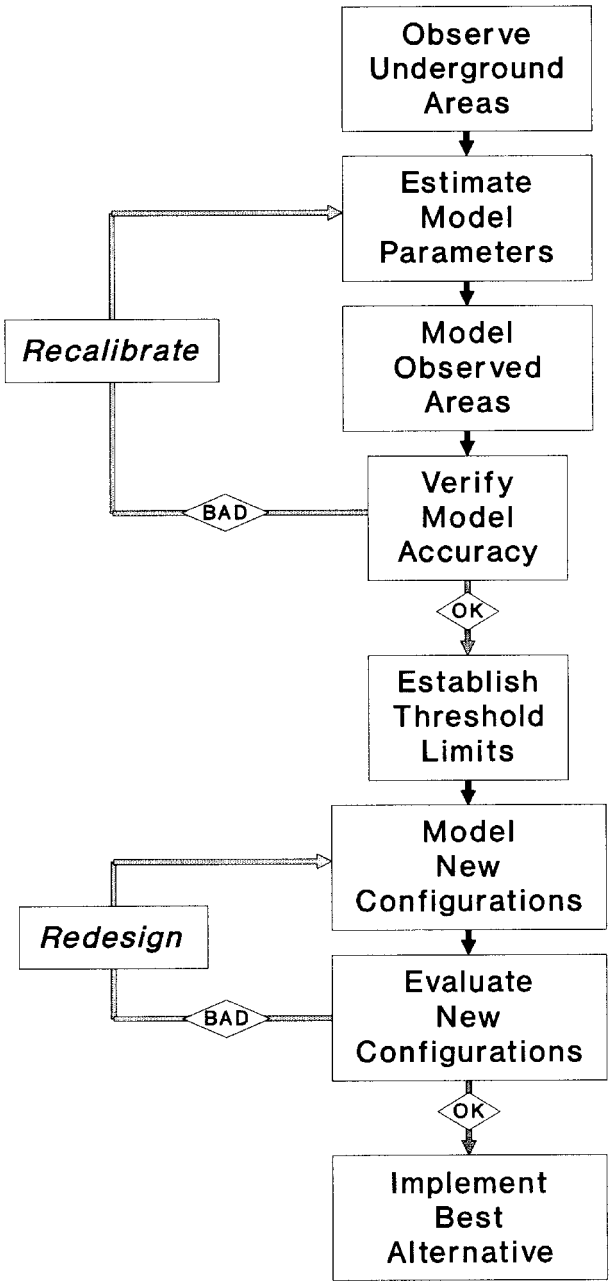

Figure 2.—Simulation process.

2. *Estimate Model Parameters:* Coal, rock, and gob properties must be established consistent with the requirements of a particular numerical method. Ideally, these properties will be based on coal and rock tests of the specific mine site. In the absence of these data, published properties of adjacent or same seam mines can be used. When no site-related data are available, general coal and mine roof rock properties can be used. Regardless of the source of data, it cannot be overemphasized that they represent only a *first estimate* of mine roof and rock properties that must be validated.

3. *Model Observed Areas:* The third step of the process involves modeling each of the areas observed underground. The properties estimated above are tested under various geometric and overburden conditions to determine their usability. Successfully modeling many areas under a variety of different conditions increases confidence in the properties used.

4. *Verify Model Accuracy:* This is the most critical step in the entire simulation process. Each of the areas modeled must be closely examined to ensure that the results correlate with observed conditions. If reasonable correlations cannot be made, the model must be recalibrated (material properties adjusted) and the process repeated. It should be noted that relating the output of numerical models (stress, convergence, etc.) to observed conditions (pillar sloughing and roof or floor deterioration) is often difficult given the complexities of the underground environment. The use of regression techniques to define actual conditions as a function of model output parameters (using the deterioration index rating system) can simplify that task.

5. *Establish Threshold Limits:* Once the accuracy of the model is verified, threshold limits delineating acceptable and unacceptable mining conditions must be established in order to evaluate the effectiveness of proposed design alternatives. Stress or convergence levels corresponding to deteriorating ground conditions can be identified. Other factors such as the extent of pillar yielding or predicted pillar, roof, and floor conditions from a more comprehensive regression analysis can also be used.

6. *Model New Configurations:* Having established an effective model and a means of evaluating the results of analyses, new mining techniques can be simulated. Generally, several alternatives are modeled under the conditions expected at the mine location where the design will be implemented.

7. *Evaluate New Configurations:* The various alternatives can be evaluated relative to the threshold limits established. For instance, if specific stress and convergence values were found to correspond to deteriorating ground conditions, an alternative

that produces levels lower than those values would be desired. However, if none of the configurations evaluated meet the threshold requirement for stable conditions, new alternatives must be developed and analyzed.

8. *Implement Best Alternative:* Once the best alternative is identified (either meeting the threshold criteria or providing the most favorable conditions), it can be *cautiously* implemented. The level of confidence in achieving a successful design is directly proportional to the breadth of the evaluation and the degree of correlation noted in the model verification process. In any event, conditions should be closely monitored as the design is implemented; any deviations from the expected behavior warrants recalibration of the model.

MINING GEOMETRY AND INITIAL STRESS

An essential element in the simulation process is creating a model grid that duplicates the in-mine geometry. The seam must be broken into elements of a size that allows the entry, crosscut, and pillar dimensions to be accurately reproduced. Seam elements must be small enough to model details of the mine geometry and produce discernable differences in performance, yet large enough to allow broad areas of the mine to be included in the simulation.

Generally, setting the element size at 1/2 the entry width (figure 3) has provided acceptable results in most coal mining applications. A 10-ft element width (for a 20-ft-wide entry/crosscut configuration) enables a large area (1,800 by 2,700 ft) to be modeled, yet provides the stress and convergence detail needed to effectively evaluate conditions. Both larger (one-entry width) and smaller (1/4-entry width) element sizes have been used out of necessity in specific applications, but are limited in application to scenarios where detail (large elements) or influence area (small elements) are not critical.

A number of other geometric guidelines have been identified that can aid in creating an effective boundary-element model:

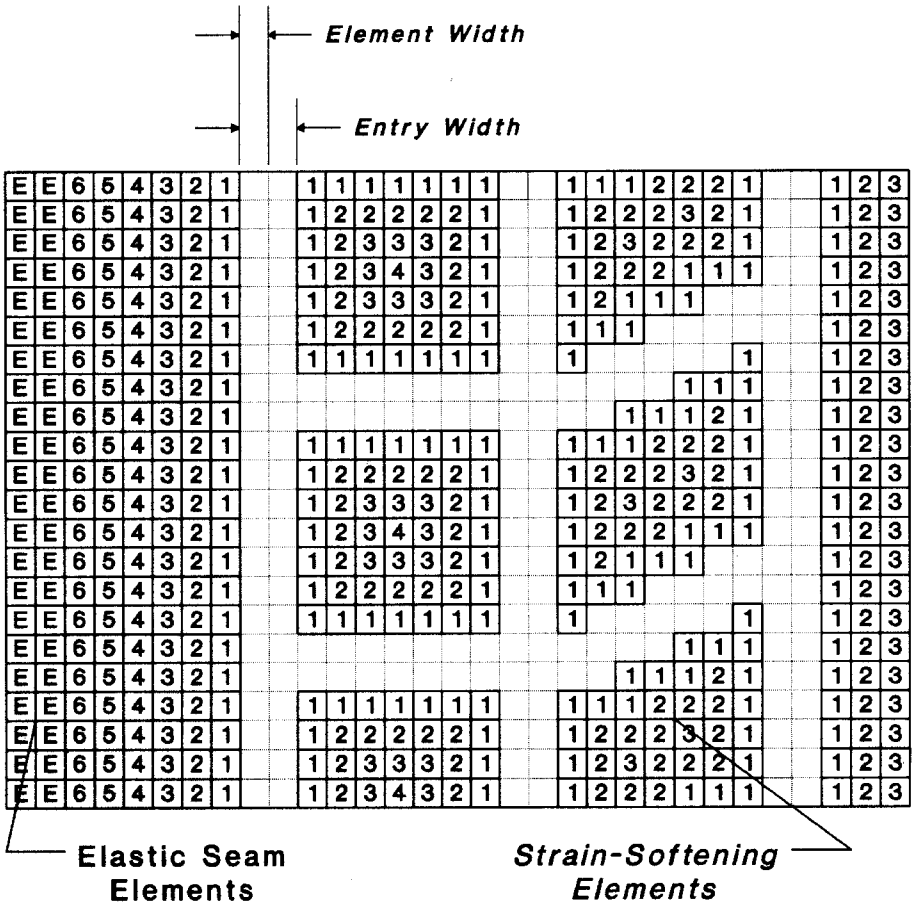

Figure 3.—Model elements and strain-softening locations.

• To the extent possible, locate model boundaries over solid coal or known stable areas to reduce the likelihood of erroneous loading conditions (resulting from the exclusion of transferred stress from adjacent yielded areas in the zone of interest).

• Orient the model such that the primary areas of interest are positioned away from the boundaries to minimize end effects.

• Known or potential yielding pillars should not contain linear-elastic elements that could erroneously affect the stress transfer to adjacent areas.

• Known or potential yielding pillars should contain an odd number of elements across the minimum dimension to ensure accurate pillar strength and peak core stress calculations.

• Care should be taken when entries or crosscuts are not oriented at 90° angles (see figure 3) to ensure that the effective widths and percent extraction match the actual mine geometry.

Initial stress conditions on the rock mass, in the absence of known high horizontal stress fields, have generally been as follows:

Szz (vertical) ' 1.1 psi per foot of depth

Sxx (x-horizontal) ' 50% of the vertical stress

Syy (y-horizontal) ' 50% of the vertical stress

These values have resulted in effective simulations of in-mine conditions in the vast majority of cases modeled, even when the influence of horizontal stress was suspected. High horizontal stress was rarely found to actually control mine conditions, and high horizontal stress values are only used when clear evidence of their existence and magnitude is available.

ROCK PROPERTIES

The rock mass properties needed for boundary-element models are minimal because the assumption of a linearly elastic material is inherent. The BESOL system requires only estimates of the modulus of elasticity and Poisson's ratio of the rock mass. Initially, it may seem that treating a complex rock structure in such a simplistic manner is not appropriate. However, considering that seam stresses are generated through massive main roof loading (generally remaining in elastic compression), it is not unreasonable to expect that an effective representation of pillar loading (the crux of a boundary-element model) would result.

The Roof Control Division uses a weighted-average technique to calculate the rock mass modulus of elasticity. As many borehole logs as possible located over areas to be modeled are examined, and the percentages of the various rock types (e.g., shale, sandstone, coal) in each core are identified (table 1). These values are averaged, multiplied by the modulus of elasticity of each rock type to calculate composite portions, then summed to estimate the rock mass modulus of elasticity. Ideally, individual strata moduli are established by site-specific tests. If those data are not available, then published data for local mine roof strata or typical rock properties must be used. It should be noted that published data for particular rock types vary widely, and some judgment is needed in selecting appropriate values. The specific rock moduli listed in table 1 have been used successfully in a number of instances when on-site data were not available.

A similar weighted-average process is recommended for the calculation of Poisson's ratio. Again, the use of site-specific data would be ideal, but estimates based on published data are generally used. Poisson's ratios ranging from 0.20 to 0.25 have been acceptable in the analyses made to date.

The properties used to define the rock mass can have a significant effect on the accuracy of a simulation. Overestimating the rock modulus results in lower pillar stresses within a panel or mined area (gob) and higher loads over the adjacent abutments due to the enhanced bridging action (less deformation) of the rock strata. Conversely, underestimating

Table 1.—Composite rock modulus calculation

Rock type	Percent in borehole					Rock modulus, psi	Composite portion, psi
	Hole No. 1	Hole No. 2	Hole No. 3	Hole No. 4	Average		
Dirt	10.84	8.07	11.51	15.64	11.52	50,000	5,750
Coal	1.52	1.60	1.34	0.96	1.36	473,000	6,409
Shale	51.15	26.86	21.79	48.22	37.01	900,000	333,090
Slate	1.18	0.78	2.54	0	1.13	1,250,000	14,125
Sandstone	22.28	28.63	23.70	26.31	25.23	2,200,000	555,060
Limestone	0	0	0	0	0	3,200,000	0
Sandy shale	11.47	31.70	36.01	7.78	21.74	1,500,000	326,100
Fireclay	1.57	2.35	3.11	1.08	2.03	900,000	18,270
TOTAL							1,258,804

$\bar{E}$ ' 1,260,000 psi

the rock modulus leads to higher panel pillar stress or gob loading in mined areas and lower stresses on the adjacent abutments.

As noted previously, the BESOL system contains a failure index (safety factor) calculation to evaluate the rock strength/stress ratios using either a Mohr-Coulomb or Hoek-Brown failure criterion. Essentially, the state of stress of a point in the rock mass is calculated in terms of 3-D principal stresses, and the "available strength" of the rock (as influenced by confinement) is compared to the existing stress level. To date, only the Mohr-Coulomb technique has been used, which requires input of cohesion, friction angle, and tensile strength of the rock (roof or floor) material. Because the analysis of the rock structure is completely elastic, exact properties (although desirable) are not required. The failure index analysis is treated in a relative manner (higher failure indices indicate a more stable condition), and the following parameters have provided reasonable results:

Tensile strength - 1,000 psi
Cohesion - 800 psi
Friction angle - 25°

The failure index has been successfully used to indicate high stress locations and the effect of mining changes to relieve those stresses. Although they can be calculated anywhere in the rock mass, failure index calculations made at the immediate roof or floor lines have been most useful. Coupling them with stress and convergence data provides a more complete picture of mine stability that can be correlated to observed or expected conditions.

COAL PROPERTIES

Establishing representative coal properties for a boundary-element analysis is the most critical step in model formulation. The need for yielding seam capability is clear to accurately simulate the complex underground environment where localized coal failure results in the redistribution and concentration of stress in adjacent areas. The strain-softening approach [Crouch and Fairhurst 1973] has been identified as a reasonable method of describing coal seam behavior. Although that concept has been widely discussed, little specific information is available concerning the actual construction of a strain-softening model.

The Roof Control Division has established a technique to make a *first approximation* of the stress and strain values needed to describe the strain-softening characteristics of a specific coal seam. As generalized in figure 4, peak and residual (postpeak) stress and strain levels are required for seam elements located at various distances from a mined area. BESOL allows up to six user-defined elements (each characterized by three stress-strain values), and model elements located farther away from a free face are treated as linearly elastic (figure 3).

Peak coal strength values are estimated at the center of each of the six yielding seam elements by the following equation:

$$S_p(i) = S_1 + (0.78 \pm 1.74\, x/h), \quad (1)$$

where $S_p(i)$ = peak strength of element (i), psi,

S_1 = in situ coal strength, psi,

x = distance from element (i) center to free face, ft,

and h = seam height, ft.

Equation 1 was based on the derivations of Mark and Iannacchione [1992] for estimating the stress gradient in the yield zone of several empirical pillar design formulas and represents an average of the Bieniawski and Obert-Duvall methods. The in situ coal strength is usually based on uniaxial compression tests of samples acquired from the mine, although published data have also been used when site-specific data were not available. Strength reduction factors of 1/5 for 2-in cubes and 1/4 for 3-in cubes have been used to estimate in situ strength from test data and have generally provided acceptable results. Figure 5 presents a summary of peak strengths measured (with borehole pressure cells) at various depths into coal pillars at three mines where pillar yielding was evident. Data are shown as a ratio of the measured peak stress to that estimated by equation 1; the majority fall within 10% of the predicted stress level. Because the seam is considered to behave elastically until peak stress is reached, the total strain at that level is simply

$$e_p(i) = S_p(i)/E, \quad (2)$$

where $e_p(i)$ = strain at peak strength of element (i), in/in,

$S_p(i)$ = peak strength of element (i), psi,

and E = coal seam modulus of elasticity, psi.

Residual (postpeak) seam stress and strain values are approximated by the following relationship:

$$S_{R1}(i) = (0.1385 \times \ln(x) + 0.413) \times S_p(i) \quad (3)$$

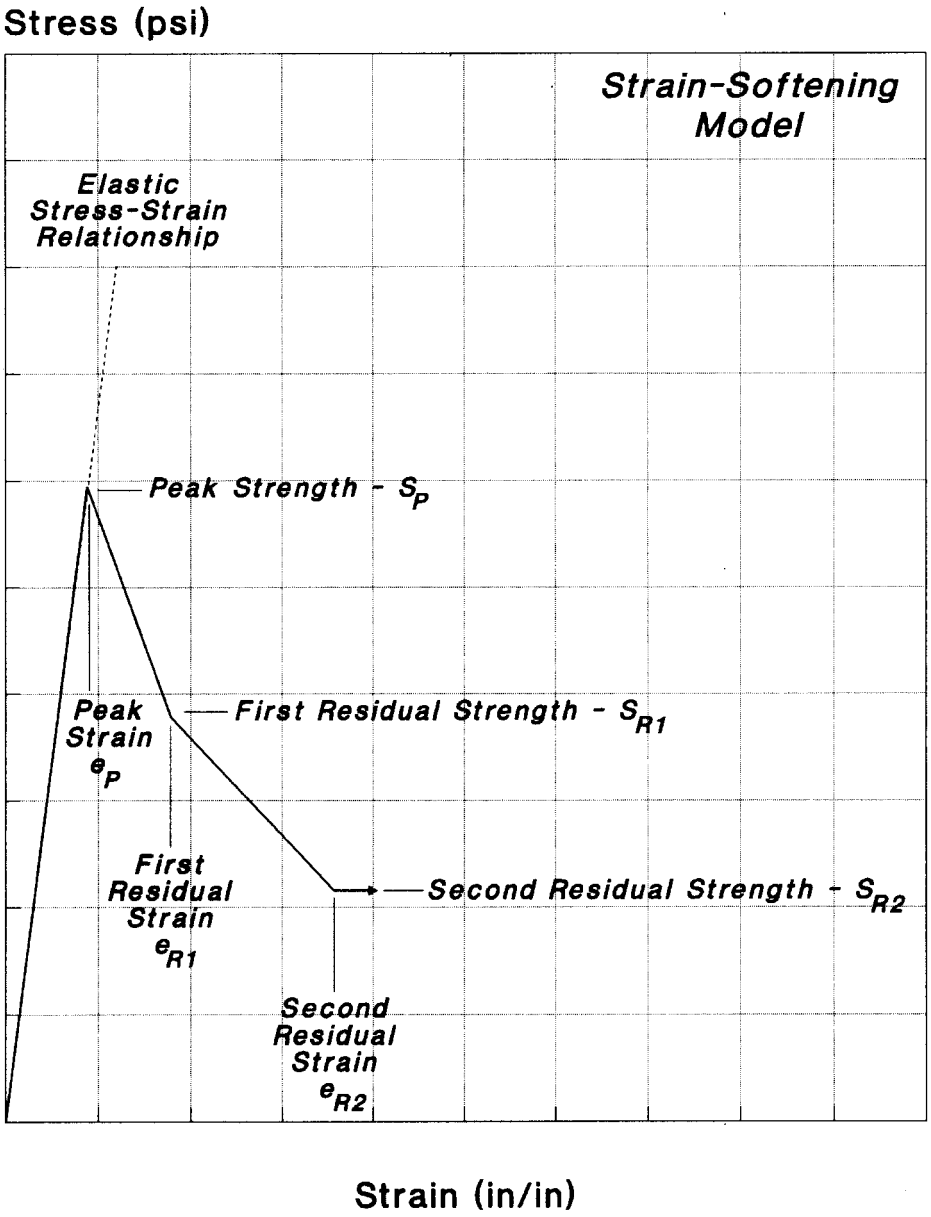

Figure 4.—General strain-softening element characteristics.

$$e_{R1}(i) = 2 \times e_p(i) \quad (4)$$

$$SR2(i) = (0.2254 \times \ln(x)) \times S_p(i) \quad (5)$$

$$e_{R2}(i) = 4 \times e_p(i) \quad (6)$$

where $S_{R1}(I)$ = first residual stress level of element (i), psi,

$e_{R1}(I)$ = strain of element (i) at first residual stress level, in/in,

$S_{R2}(I)$ = second residual stress level of element (i), psi,

$e_{R2}(I)$ = strain of element (i) at second residual stress level, in/in,

and x = distance from element (i) center to free face, ft.

These relationships were patterned after the load/deflection response of coal samples under uniaxial testing, yield pillar stress and entry convergence measurements made at one mine site, and the assumption that at increasing depth into the pillar core a higher residual strength would be maintained.

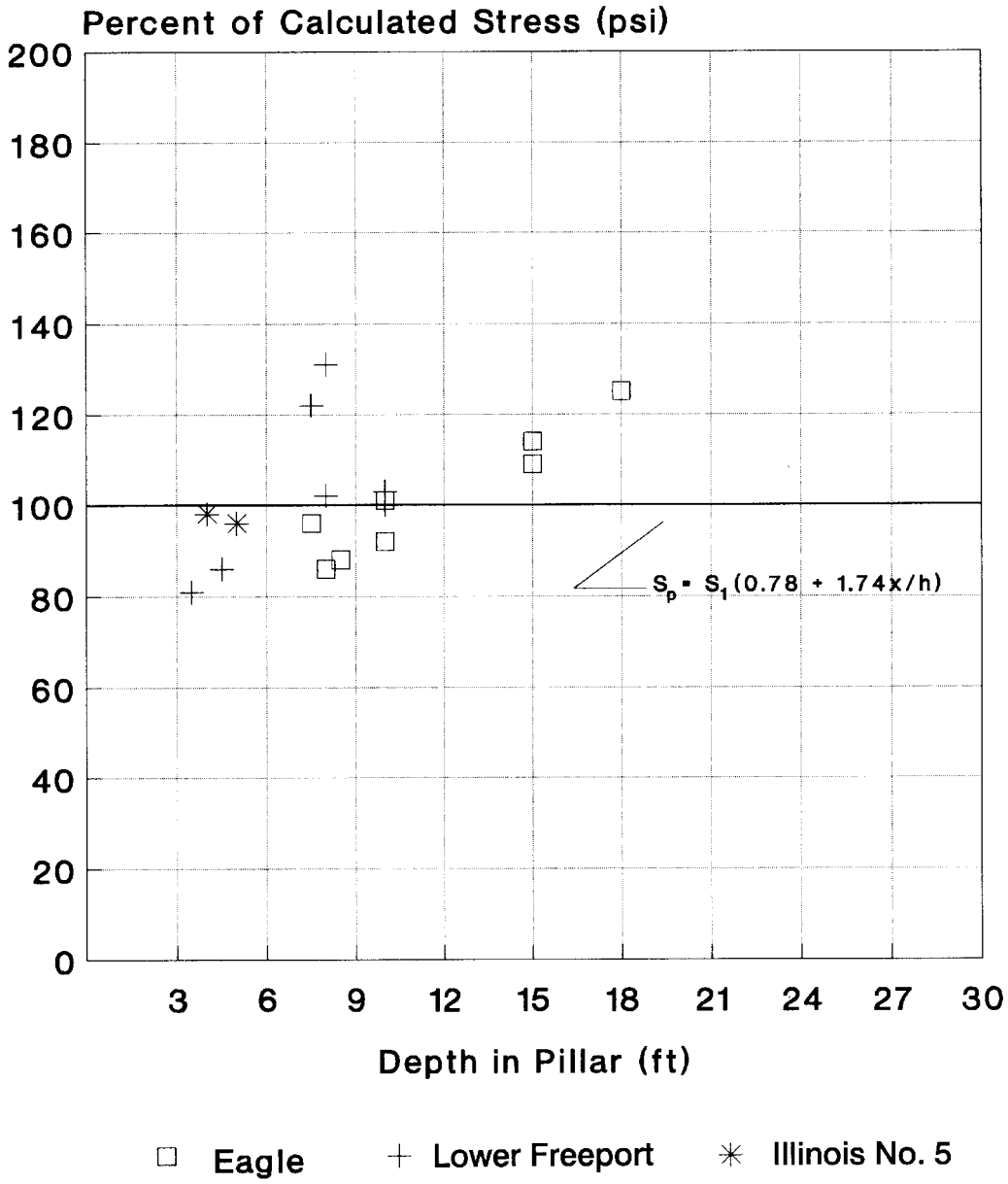

Figure 5.—Measured versus calculated peak coal strength.

Figure 6 presents a summary of residual stress levels measured at various depths at four mines where pillar yielding was monitored. The data are illustrated as a percentage of measured peak stress and compared to levels predicted by the above equations. The R1 levels represent the initial drop in stress once the peak has been reached; the R2 values indicate the final magnitude after substantial convergence. Both are difficult to identify because deformation plays a significant role in the unloading process; however, figure 6 represents a best estimate of those stress levels for the pillars monitored.

Figure 7 illustrates a family of six curves representing a strain-softening model with an element size of 10 ft, a seam height of 2.8 ft, an elastic modulus of 500,000 psi, and an in situ coal strength of 967 psi. Curve No. 1 represents the behavior of free-face or pillar perimeter elements; the remaining curves represent the stress-strain relationship of elements located successively deeper into the pillar core.

The BESOL system also requires estimates of the seam shear modulus (G) and similar shear stress-strain characteristics for the six yieldable elements described above. These geotechnical

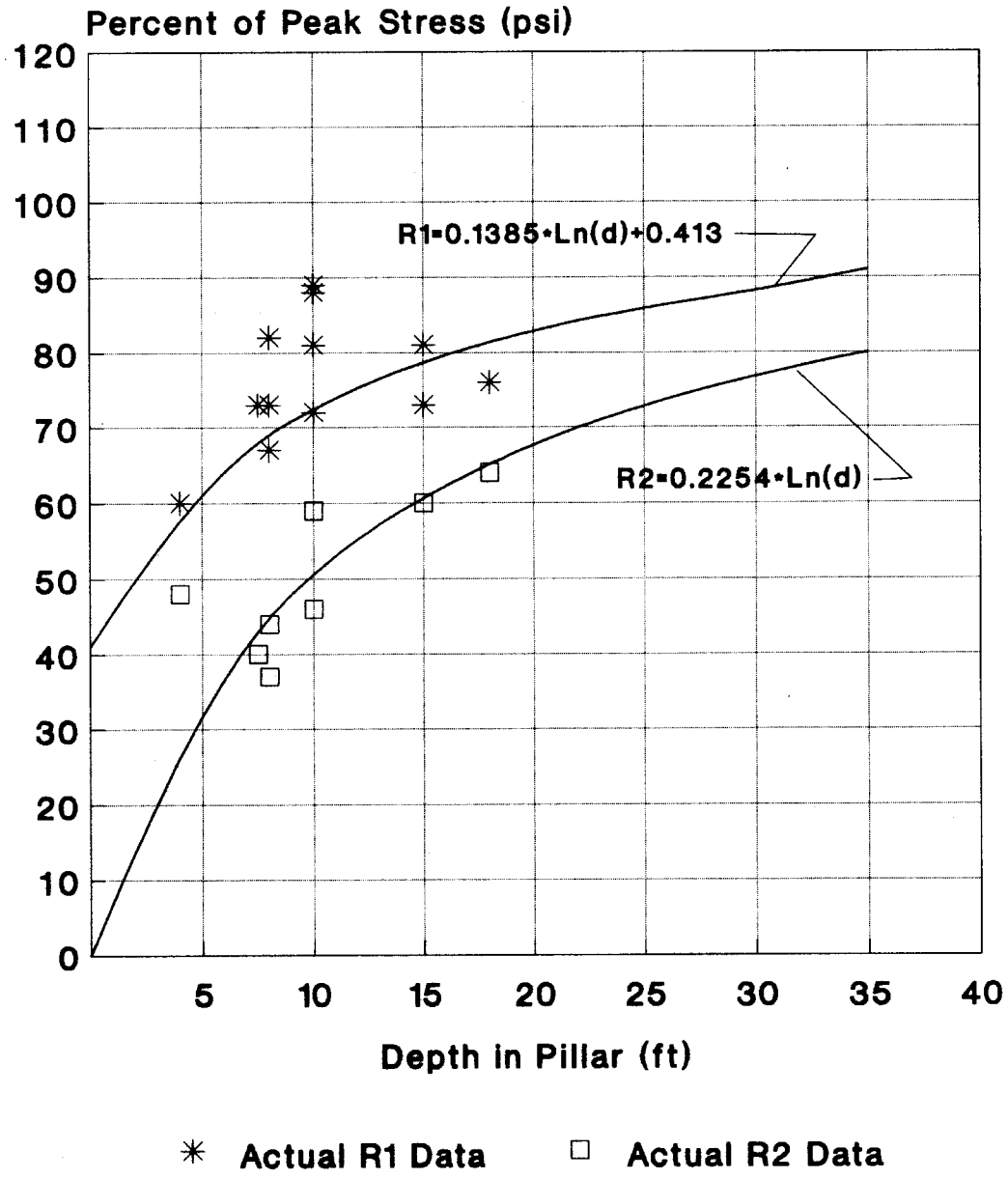

Figure 6.—Measured versus calculated residual strength.

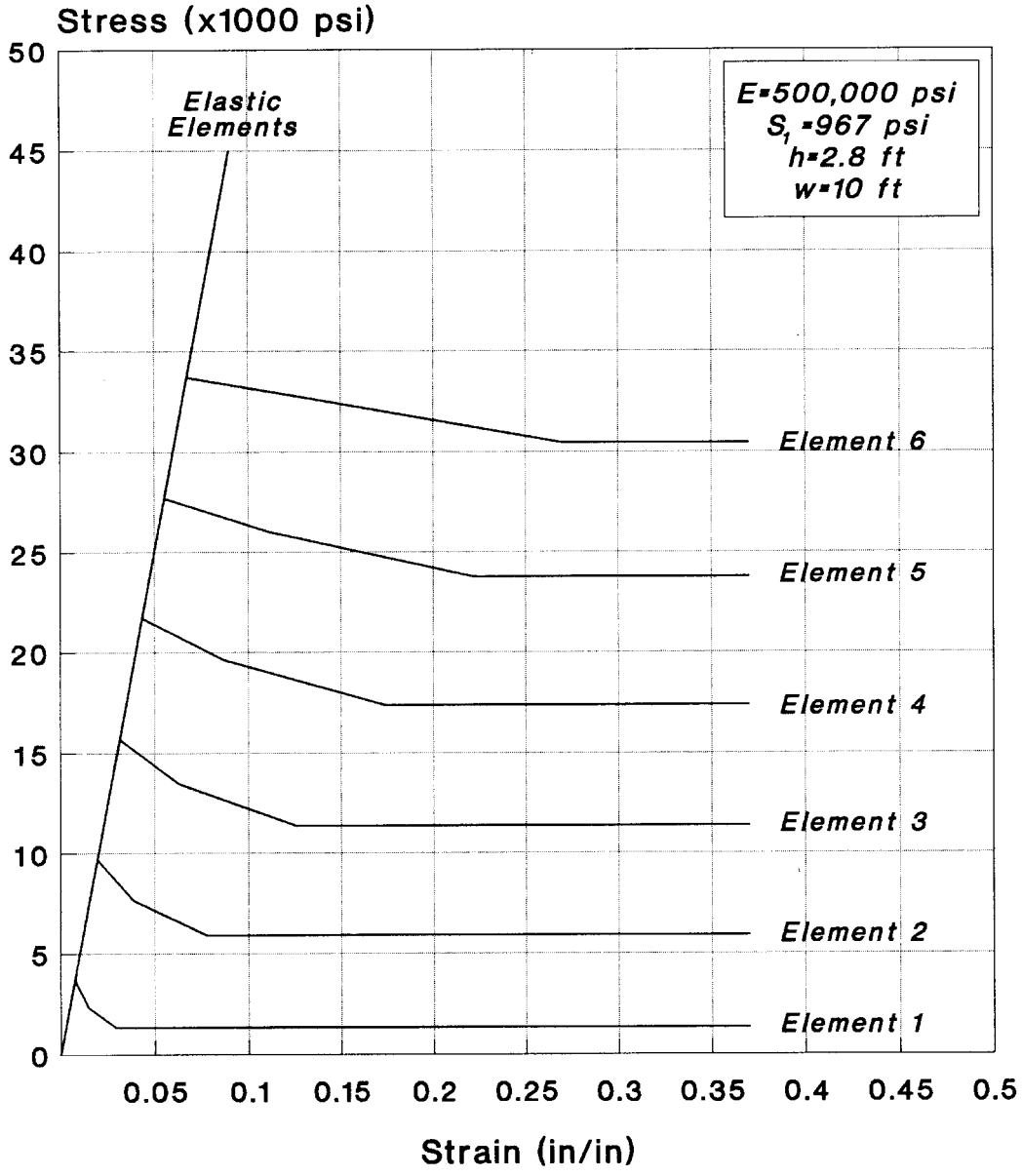

Figure 7.—Typical strain-softening seam behavior.

data are rarely available, and estimates (using the previously described procedure) based on a shear modulus equal to 1/2 to 1/3 of the elastic modulus and shear strengths of 1/2 to 1/3 of the strain softening values have been used.

It must again be emphasized that, although the methodology described above has been successfully used to estimate coal strain-softening properties, the properties generated are only a *first approximation* that must be verified for accuracy. Although in situ measurements have generally validated properties assigned to near-excavation locations, peak and residual stress levels deeper than 20 ft into a pillar or solid coal (where yielding rarely occurs) are largely unverified. Further, the procedure has been applied only to a limited number of coal seams, none of which experienced bump problems. The application of this technique to bump coal is not recommended because the strength increase due to confinement would likely exceed that predicted by the peak stress equations.

The suitability of assigned coal properties can be assessed by comparing the simulation output to observed pillar conditions. Test models should include underground areas (varying depths and pillar sizes) where definite observed pillar behavior can be isolated. For instance, if a model with 8-ft-wide elements predicts corner yielding, significant sloughing and crushing for a length of 8 ft from the pillar corner should be obvious. A similar condition would be expected along the sides of pillars if perimeter yielding were projected. In general, more observed pillar deterioration than that projected by the model suggests that the coal strength has been overestimated; less sloughing than predicted indicates that it has been underestimated. There are occasions, however, where the element size itself can contribute to erroneous interpretations. A model using 10-ft elements may indicate elevated stress at the pillar corners, but no yielding. Underground observations of 4-ft crushed zones at the pillar corners may suggest that the model coal strength has been overestimated. Remodeling the area using 4-ft elements (with corresponding recalculation of element properties) may in fact result in the prediction of corner yielding that would match the in-mine conditions.

When constructing calibration models to verify coal strength, it is essential that:

- The element size selected is appropriate to illustrate phenomena (yielding) observed underground; and
- Element properties are recalculated when element sizes are changed; smaller elements have lower strength values than larger ones because of their proximity to the free face.

GOB PROPERTIES

When numerical models contain large mined areas, such as longwall or pillar line gobs, some mechanism must be employed to simulate caving and stress relief associated with those areas. Without it, the full weight of the overburden would be transferred to adjacent areas and result in a significant overestimation of abutment loads. The stress relief process is complex and comprises caving, bulking, and subsequent compaction of the gob material. Although a number of investigators, including Pappas and Mark [1993], have evaluated the behavior of gob material, little published data exist regarding the simulation of caving in 3-D boundary-element numerical models.

The BESOL system provides a fill material that has been used to absorb a portion of the gob loads and provides a measure of stress relief associated with caving. The stress-strain relationship for the fill material is based on the work of M. D. G. Salamon and is of the form [Crouch Research, Inc. 1988]:

$$F_n = a \left(e_n / (b - e_n), \right. \quad (7)$$

where F_n = normal stress on the fill element,

e_n = normal strain of the fill element,

b = limiting value of normal strain (total compaction), and

a = stress to compress fill 1/2 of b.

For a first approximation, values for the necessary constants have been estimated as:

a = 100 psi
b = 0.50 in/in

Figure 8 illustrates the relatively soft stress-strain response of backfill using these parameters. That material was tested in a number of general scenarios; resultant abutment loads were compared with those predicted by the inverse square decay function used by Mark [1990] in the Analysis of Longwall Pillar Stability (ALPS) methodology. As typified by figure 9, a reasonable agreement in resultant abutment stress distributions was found. The peak stress of the BESOL model exceeds that of the inverse square decay function; the average stress over the first 150 ft of the abutment (usually the zone of concern) is nearly identical. It appears that the use of a relatively soft backfill compensates for the tendency of boundary-element models to distribute abutment loads over a wide area and results in a reasonable approximation of near-gob stresses. Fill material of this type has been placed in gob areas during the BESOL simulation of nine mines (starting 20-30 ft from solid coal to allow an area of hanging roof) that have been successfully evaluated.

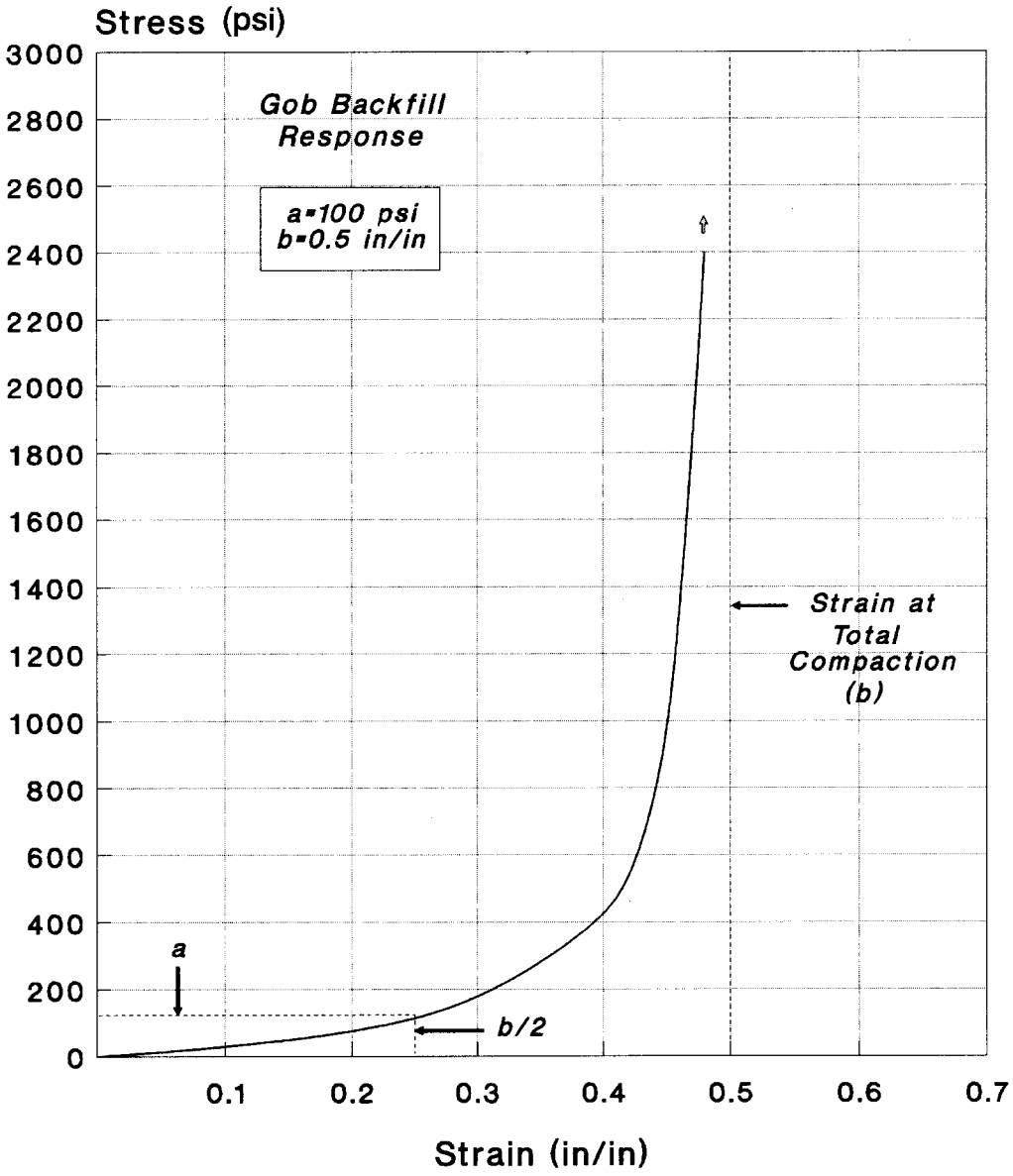

Figure 8.—BESOL strain-hardening backfill behavior.

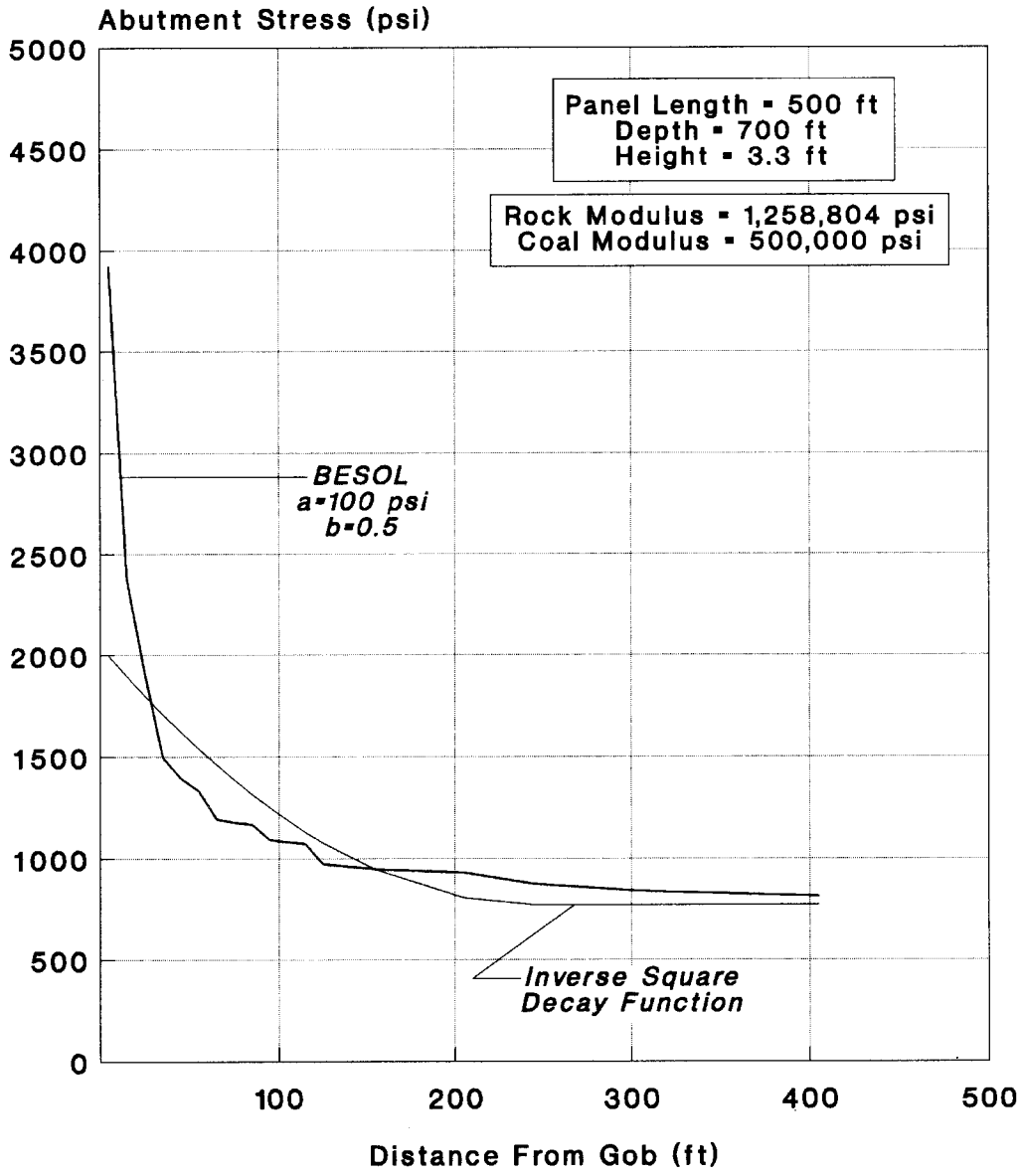

Figure 9.—BESOL versus inverse square decay function.

As with the other material properties discussed in this paper, the suitability of gob backfill based on the above or any other parameters must be verified. Obviously, the use of backfill that is too stiff will result in excessive gob loading and reduced abutment loads. Conversely, a gob material that is too soft will generate excessive abutment loads and low-gob stress. The modulus of elasticity of the rock mass and other geometric parameters (depth, panel width, etc.) can have a significant impact on backfill loading and must be considered. Examining backfill stress in gob areas can indicate the amount of relief simulated by the model and can be compared to known or anticipated cave heights associated with those areas.

SUMMARY OF PROPERTIES

In the process of simulating ground conditions at mines throughout the United States (12 coal seams in 5 States), a host of coal and rock properties have been generated. Table 2 summarizes the in situ coal strength, coal modulus of elasticity, and rock moduli of elasticity used in 18 successful evaluations. The mining depth of each simulation is also shown in the table. The data are presented for reference purposes and illustrate the variation in properties that can be expected at different sites.

Table 2.—Successfully applied coal and rock properties

State and coal seam	Mining depth, ft	In situ coal strength, psi	Coal modulus of elasticity, psi	Rock modulus of elasticity, psi
PA:				
Lower Freeport	420	[1]462	[1]550,000	[2]1,000,000
Upper Freeport	700	[1]405	[1]200,000	[1]590,000
Upper Freeport	360	[1]775	[1]200,000	[1]740,000
Pittsburgh	950	[2]790	[2]350,000	[2]2,100,000
Pittsburgh	650	[2]900	[2]500,000	[2]3,280,000
Pittsburgh	575	[2]790	[2]350,000	[2]2,140,000
Lower Kittanning	375	[2]679	[2]300,000	[2]1,850,000
WV:				
Cedar Grove	900	[1]705	[2]500,000	[2]1,800,000
Dorothy	150	[1]290	[1]121,000	[2]910,000
Eagle	950	[1]712	[1]490,000	[1]880,000
Eagle	850	[1]850	[1]500,000	[1]810,000
Lower Lewiston	260	[1]583	[1]200,000	[2]2,400,000
Sewell	470	[1]312	[1]250,000	[2]1,400,000
KY:				
Elkhorn No. 3	420	[1]951	[1]548,000	[2]1,750,000
Hazard No. 4	900	[1]967	[2]500,000	[2]1,260,000
Hazard No. 4	950	[2]967	[2]500,000	[2]1,260,000
IL:				
Illinois No. 5	700	[2]620	[2]330,000	[2]1,000,000
AL:				
Blue Creek	1,200	[2]750	[2]580,000	[2]1,440,000

[1]Based on site-specific tests.
[2]Estimated from published data provided by the mine or found in literature reviews.

DETERIORATION INDICES AND ANALYSIS

As mentioned previously, the most critical phase of the simulation process is verifying the accuracy of a model through correlation with actual underground conditions. To aid in that exercise, a set of deterioration indices was established to quantify pillar, roof, and floor behavior. Observed sites are assigned a numerical rating on a scale of 0 to 5 (0 is the best condition; 5 is the most severe) in each of the three categories. The deterioration index levels are reasonably well defined to minimize subjectivity of observations and promote consistency in ratings from site to site.

The pillar deterioration index (PDI) establishes observable sloughing levels that can be directly related to numerical model projections. A rating of 1 indicates corner crushing for a distance equal to one element width (usually 1/2-entry width) in the boundary-element model. A rating of 2 indicates some perimeter sloughing, but to a depth of less than one element width. This corresponding model would indicate yielding of some, but not all, of the perimeter seam elements. At the 2.5 level, sloughing is severe enough to cause concern over the stability of the area. A PDI of 3.5 represents a situation where

sloughing caused widening of the entry to a point that supplemental support (cribs or posts) was required to narrow the roadway. A corresponding model would indicate yielding of all perimeter elements and elevated pillar core stresses. PDIs of 4 and 5 represent progressively more severe conditions. A model response equivalent to a level 4 would indicate deeper pillar yielding and core stresses approaching the maximum capacity; a level of 5 indicates total pillar yielding and elevated convergence.

Pillar deterioration index (PDI)

0	Virtually no sloughing
1.0	Corner sloughing
2.0	Light perimeter sloughing
2.5	Onset of pillar stability concerns
3.0	Significant perimeter sloughing
3.5	Supplemental support required
4.0	Severe perimeter sloughing
5.0	Complete pillar failure

The roof deterioration index (RDI) defines a rating scale to quantify the condition of the roof strata in observed areas. Unlike the PDI, however, roof deterioration cannot be directly correlated to model output. The levels were established to correspond to progressively more significant observable phenomena ranging from roof flaking or sloughing (level 1) to widespread and massive roof falls (level 5). The severity of each feature can be identified within a one-point band. For instance, areas with only a hint of roof cutters would be rated at 1.6; those containing many severe cutters (a situation causing roof stability concerns) would receive a 2.5 rating. A roof deterioration index of 3.5 corresponds to conditions where supplemental support was required to maintain stability.

Roof deterioration index (RDI)

0	Virtually no deterioration
1.0	Flaking or spalling
2.0	Cutter roof
2.5	Onset of roof stability concerns
3.0	Broken roof
3.5	Supplemental support required
4.0	Significant roof falls
5.0	Widespread and massive roof falls

The floor deterioration index (FDI) provides a measure of mine floor stability relative to fracturing and the level of heave experienced. Like the RDI, this index cannot be directly correlated to the model output, and the established levels represent progressively more serious floor conditions. An FDI of 2.5 represents the occurrence of heave that causes concern over floor stability; a level of 3.5 indicates a condition that impedes passage and requires grading to maintain an active travelway.

Floor deterioration index (FDI)

0	Virtually no deterioration
1.0	Sporadic cracks
2.0	Consistent localized cracks
2.5	Onset of floor stability concerns
3.0	Widespread cracks and obvious heave
3.5	Travel impeded; grading required
4.0	Significant floor displacement
5.0	Complete entry closure

The deterioration indices have been effectively used to describe in-mine ground conditions and to correlate BESOL output data to those observations. While simulation output such as stress and convergence can often be directly related to in-mine conditions, many instances arise where the combined influence of a number of factors affects ground behavior. To better establish those relationships and provide an effective means of evaluating potential design alternatives, a multiple linear regression can be used to relate model output to observed (deterioration index) conditions.

Table 3 presents a partial listing of BESOL output (stress, convergence, and failure index (FI) at the immediate roof line) and deterioration indices for a number of areas modeled and observed during an actual mine analysis. Other BESOL output (i.e., horizontal stress or displacement) could be included if applicable to a particular situation, but the three parameters listed are those routinely used. After model and observation data for all of the evaluated areas are compiled, multiple linear regression analyses are performed to define each deterioration index as a function of model output. In the sample instance in table 3, the various deterioration indices were related to maximum stress, maximum convergence, and minimum failure index at the roof line, and the resultant regression equations and correlation coefficients are listed.

Once the model accuracy is verified by comparing predicted to observed pillar yielding, examining the regression correlation coefficients, and using the regression equations to back-calculate deterioration indices for the observed (modeled) areas, design alternatives can be modeled and expected conditions predicted. Table 4 contains projected deterioration indices at a critical pillar line location for various pillar sizes and depths of

cover as predicted by BESOL output and the verified regression equations. The difference in expected conditions with each design alternative is clear.

The deterioration index/regression equation technique has proved to be a viable method of verifying numerical model accuracy and evaluating the potential of design alternatives *provided that* relatively consistent mining conditions exist. When changing roof, pillar, or floor strengths are encountered, the usability of the regression technique may be greatly reduced. Further, the relationships established are based on strata reaction at a particular mine, and only those observed (which are limited by current mine design and environment) can be included in the database. This is a particular concern when the use of yield pillars as an alternative configuration is considered, but no complete pillar yielding is evident at the mine.

The Roof Control Division is currently exploring the use of normalizing parameters in the regression analysis to alleviate these difficulties. Factors such as in situ coal strength and seam height (for the PDI), a roof rock rating such as the Coal Mine Roof Rating (CMRR) [Molinda and Mark 1993] for the RDI, and a floor characterization number (for the FDI) are being evaluated to determine their usefulness in the regression analysis to buffer the variations found within a given mine and also between mines. If successful, the resultant technique could enhance individual mine analyses and allow the experience of many mines to be used.

Table 3.—Partial BESOL/deterioration index listing and regression equations

Location and entry	BESOL output			Deterioration indices					
				Observed			Back-calculated		
	Maximum stress, psi	Maximum convergence, ft	Minimum failure index (FI)	PDI	RDI	FDI	PDI	RDI	FDI
Face area:									
1	4,000	0.113	1.04	1.5	1.5	0.0	1.5	1.2	0.2
2	6,800	0.195	1.09	2.0	1.8	0.3	2.5	2.4	1.2
3	8,100	0.251	0.96	3.5	3.0	1.0	3.0	2.9	1.7
4	8,800	0.289	0.89	4.0	4.2	2.5	3.3	3.3	2.0
5	8,800	0.307	0.87	4.0	3.5	4.0	3.3	3.4	2.1
1 crosscut outby:									
1	3,100	0.083	1.11	1.2	1.5	0.0	1.1	0.9	0.0
2	5,400	0.161	1.16	1.5	1.5	0.0	2.0	1.9	0.8
3	7,000	0.207	1.11	2.0	2.0	0.5	2.6	2.5	1.3
4	7,500	0.230	1.02	3.0	3.0	1.0	2.8	2.7	1.5
5	7,500	0.223	0.94	3.0	3.0	3.0	2.7	2.6	1.4
3 crosscuts outby:									
1	2,710	0.063	1.25	1.0	0.5	0.0	1.0	0.7	0.0
2	3,900	0.089	0.93	1.5	0.8	0.0	1.3	1.1	0.0
3	6,000	0.150	1.16	1.5	1.5	0.2	2.2	2.0	0.9
4	7,000	0.182	1.13	2.0	2.0	1.0	2.5	2.4	1.2
5	7,300	0.204	1.21	3.0	2.5	2.0	2.7	2.6	1.4
3-Right:									
2	2,240	0.059	1.53	1.0	0.5	0.0	1.0	0.7	0.0
4	2,560	0.070	1.41	1.4	1.0	0.0	1.1	0.8	0.0
5	2,820	0.072	1.45	1.5	1.4	0.1	1.2	0.9	0.0
1-Right:									
2	1,530	0.040	2.13	1.0	0.2	0.0	1.0	0.6	0.0
4	1,700	0.047	1.91	1.0	1.0	0.0	1.0	0.6	0.0
5	1,780	0.047	2.00	1.0	1.0	0.0	1.0	0.7	0.0

PDI ' 0.000268 (STR % 3.259622 (CONV % 0.379665 (FI & 0.383740 r^2 ' 0.79

RDI ' 0.000263 (STR % 4.603502 (CONV % 0.309200 (FI & 0.643870 r^2 ' 0.80

FDI ' 0.000170 (STR % 6.094244 (CONV % 0.600442 (FI & 1.82412 r^2 ' 0.60

Table 4.—Full pillaring BESOL output and predicted deterioration index

Pillar size (ft), depth, and location	Maximum stress, psi	Maximum convergence, ft	PDI	RDI	FDI
50 by 50 (900-ft depth):					
1	[1]8,300	[1]0.291	[2]3.0	[2]3.1	[3]1.7
2	[1]8,200	[2]0.247	[2]3.1	[2]3.1	[3]1.9
3	[3]5,900	[2]0.185	[3]2.1	[3]2.0	[3]0.8
4	[3]5,600	[3]0.161	[3]2.2	[3]2.0	[3]1.0
40 by 40 (900-ft depth):					
1	[1]9,690	[1]0.385	[1]3.8	[1]4.0	[2]2.7
2	[1]9,690	[1]0.343	[1]3.8	[1]3.9	[2]2.6
3	[1]8,700	[2]0.245	[2]3.0	[2]3.0	[3]1.6
4	[1]8,300	[2]0.230	[2]3.1	[2]3.0	[3]1.7
40 by 40 (800-ft depth):					
1	[1]9,690	[1]0.305	[1]3.5	[1]3.6	[3]2.2
2	[1]9,690	[1]0.269	[1]3.6	[1]3.5	[3]2.2
3	[2]6,800	[2]0.198	[3]2.4	[3]2.3	[3]1.0
4	[2]6,600	[2]0.182	[2]2.5	[3]2.4	[3]1.3
40 by 40 (600-ft depth):					
1	[2]7,300	[2]0.204	[2]2.6	[2]2.5	[3]1.2
2	[2]7,150	[3]0.171	[2]2.7	[2]2.5	[3]1.4
3	[3]3,500	[3]0.095	[3]1.2	[3]1.0	[3]0.0
4	[3]3,400	[3]0.087	[3]1.3	[3]1.0	[3]0.1
40 by 30 (400-ft depth):					
1	[3]4,400	[3]0.116	[3]1.5	[3]1.3	[3]0.2
2	[3]4,200	[3]0.098	[3]1.4	[3]1.2	[3]0.1
3	[3]2,660	[3]0.063	[3]1.0	[3]0.7	[3]0.0
4	[3]2,320	[3]0.060	[3]1.1	[3]0.8	[3]0.0

[1]Severe conditions.
[2]Borderline conditions.
[3]Desirable mining conditions.

CASE STUDY

An investigation was conducted at a coal mine in eastern Kentucky to determine the cause of a roof fall and deteriorating ground conditions that were encountered on a full pillaring section. The mine is located in the Hazard No. 4 Seam and has a mining height of 32-40 in. Figure 10 presents an illustration of the 1-Left Mains in the vicinity of the roof fall. These mains were developed as a five-entry system on 50- by 60-ft centers with 20-ft-wide entries and crosscuts. Panels were driven to the right and retreated as the mains were advanced (13 panels total). Following development of the mains (and panels) to the property boundary, retreating of those pillars was initiated. As figure 10 illustrates, a roof fall occurred one crosscut outby the pillar line as the 18th row of blocks was being extracted. Cover at the face was about 800 ft, but ranged from 480 ft near the mouth of the section (about 2,400 ft outby) to over 950 ft several hundred feet inby and to the right of the fall. The immediate roof strata were composed of a 15-ft-thick laminated shale and were overlain by a 20-ft-thick sandstone layer. Roof support was provided by 4-ft-long fully grouted bolts installed in a 4- by 4-ft pattern throughout the mains.

Observations were made throughout the 1-Left Mains to characterize ground conditions under various depths of cover and degrees of gob influence. Significant deterioration (heavy pillar sloughing, cutters, and broken roof zones) was noted in the face area; conditions were most severe in the immediate vicinity of the roof fall. Outby the face, conditions gradually improved, although the right side of the mains consistently showed heavier deterioration than the left side. The most significant conditions noted in the outby area corresponded to zones of heavier cover, suggesting that overburden depth and the adjacent gob areas contributed to the deteriorating conditions. Detailed deterioration index ratings were made throughout the observed areas to quantify the roof, floor, and pillar behavior. The data presented in table 3 represent a partial listing of these ratings in a number of entry locations (crosscut conditions were also quantified and used in the analysis). Higher PDI, RDI, and FDI levels correspond to more severe deterioration, which were observed in the face area and along the right side of the mains. Cover at the face was about 800 ft and about 650 ft and 480 ft over the 3-Right and 1-Right outby

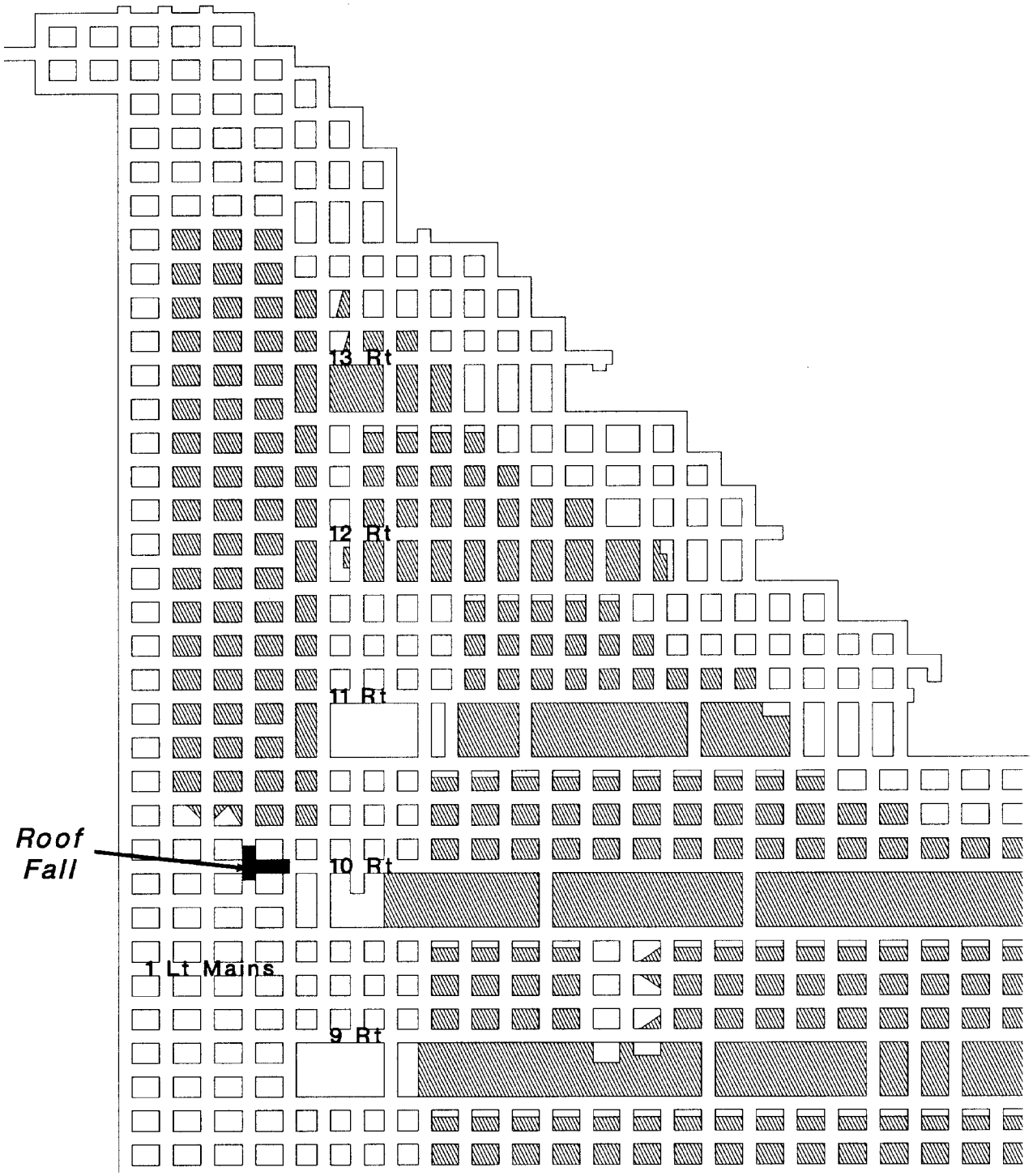

Figure 10.—Case study: partial mine map of pillaring section - roof fall area.

areas, respectively, where conditions were much improved. Figure 11 presents a composite deterioration index drawing of conditions observed at and just outby the face, illustrating the concentration of deterioration in the vicinity of the roof fall and along the right side of the section.

A series of three BESOL models was subsequently created to simulate conditions in the areas observed during the underground investigation. The first model (covering the area shown in figure 10) was used to simulate mining at the time of the roof fall and also at inby and proposed outby face positions

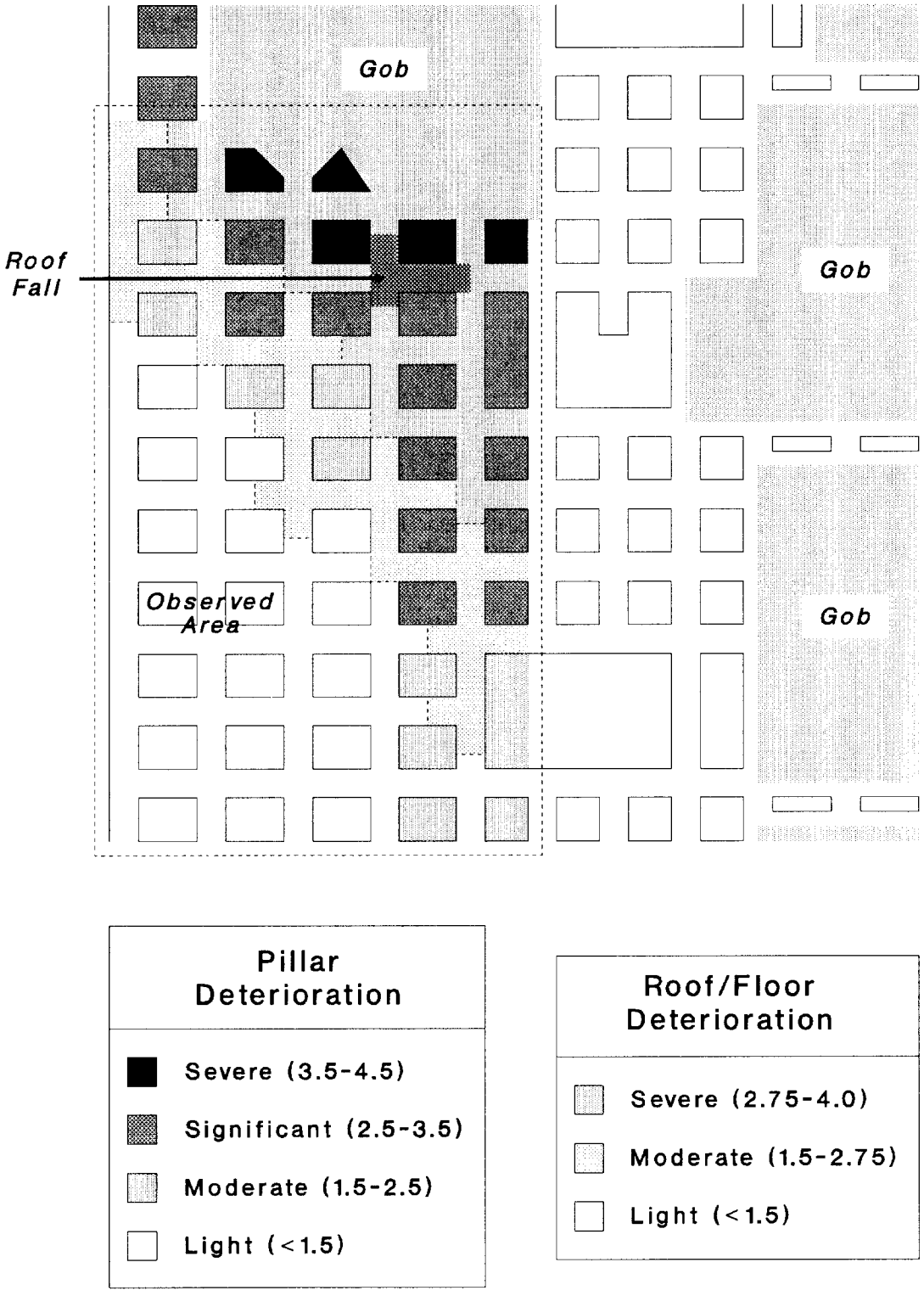

Figure 11.—Case study: observations on pillaring section - roof fall area.

where cover was approximately 800 ft. Additional models were constructed of the outby areas (3-Right (650-ft cover) and 1-Right (480-ft cover)) to provide model verification under significantly differing conditions. Vertical stress applied to the models equaled 1.1 psi per foot of depth, and a horizontal stress of 1/2 the vertical stress was assumed in both the x and y directions. The element size used in the simulations was 10 ft, or 1/2 the 20-ft-entry width.

A composite rock modulus of 1,260,000 psi was based on data obtained from four boreholes in the vicinity, as shown in table 1. The individual rock moduli were estimated from published data for the specific strata contained in each borehole. A Poisson's ratio of 0.21 and the default Mohr-Coulomb properties (cohesion ' 800 psi, friction angle ' 25°, and tensile strength ' 1,000 psi) were used because no site-specific data were available.

Coal properties were based on an in situ strength of 967 psi (site-specific coal strength data were provided by the mine); the peak and residual strength levels were calculated as outlined previously in this paper. A seam height of 2.8 ft was used, and a coal modulus of elasticity of 500,000 psi was assumed. The stress-strain curves of figure 7 represent the strain-softening model used in the analysis. Shear stress-strain properties were based on a shear modulus of 200,000 psi (0.4E).

Gob caving was simulated using the Salamon backfill discussed earlier with the constants a ' 100 psi and b ' 0.50. The comparison of abutment loading between BESOL and the inverse square decay function of figure 9 was based on the rock mechanics parameters used in this simulation.

Maximum pillar stress, maximum roof/floor convergence, and minimum failure index values were determined from the 3 models for 37 locations (entries and crosscuts) corresponding to the observed areas. The stress and convergence data compiled indicate the highest levels found in or adjacent to the 37 locations; the failure index values represent the lowest levels detected at the roof line in each area. A portion of these data (entry locations) is listed in table 3. A series of multiple linear regression analyses was made to relate the deterioration indices observed to the BESOL data and resulted in the equations also listed in table 3. The R-squared values for the PDI (0.79) and the RDI (0.80) were very good, but marginal for the FDI (0.60). It should be noted that the characterization of floor conditions was not a primary concern during the investigation, but sketchy data acquired were used to illustrate the process. The BESOL output was then inputted into the regression equations to predict (back-calculate) deterioration indices for the observed locations; these values describing entry conditions are also listed in table 3. Most of the predicted PDI and RDI levels match the observed data fairly well, and the trend of higher deterioration indices in areas of more severe conditions was evident, even with the FDI.

Figure 12 presents a composite of maximum pillar stress and convergence levels predicted by the BESOL model of the roof fall site. Note the correlation of BESOL stress and convergence with the degree of deterioration observed underground. The zone of high convergence (>0.25 ft) and stress (>9,500 psi) encompasses the area of deteriorating conditions at the pillar line, including the roof fall. Lower stress and convergence levels also correspond to zones of lesser deterioration, and the more severe conditions predicted on the right side of the mains (indicating the influence of the adjacent gob) also match the conditions observed underground. These correlations, coupled with the good fit of the regression analysis (deterioration indices), confirmed the accuracy of the model (and properties used) to simulate conditions at the mine. Confidence was further enhanced by an evaluation of the BESOL model with a face position several crosscuts inby the roof fall. The results showed significantly lower stress and convergence levels in the face area that correlated to the better mining conditions actually encountered.

It was concluded that the roof fall (and deteriorating conditions) resulted from a combination of stresses from the active and adjacent gobs overriding the pillar line (yielding) and focusing outby the face. The small pillar size employed (30 by 40 ft) on the mains, the lack of protection provided by the combination of chain and barrier pillars from the adjacent gob, and the depth of cover (>800 ft) contributed to the problems encountered.

A series of additional models was created to evaluate the performance of various pillar sizes at different mining depths that would be encountered. Figure 13 illustrates the pillaring plan to be implemented using a 200-ft barrier between adjacent panels that would be roomed and retreated along with the panel being extracted. Stresses and convergences were examined at four entry locations near the face (during retreat of the second panel), as illustrated in figure 14. Threshold levels delineating expected conditions (from the 1-Left models) were established as follows:

Severe conditions:

Stress > 8,000 psi; convergence > 0.25 ft
PDI $ 3.5; RDI $ 3.5; FDI $ 3.5

Borderline conditions:

Stress ' 6,500 to 8,000 psi; convergence ' 0.18 to 0.25 ft
PDI ' 2.5 to 3.4; RDI ' 2.5 to 3.4; FDI ' 2.5 to 3.4

Desirable mining conditions:

Stress < 6,500 psi; convergence < 0.18 ft
PDI < 2.5; RDI < 2.5; FDI < 2.5

It was predetermined that good (desirable) mining conditions should exist at locations 3 and 4 since no supplemental supports (posts) would be installed in those areas. Borderline conditions could be tolerated at locations 1 and 2 (posts are set in this area),

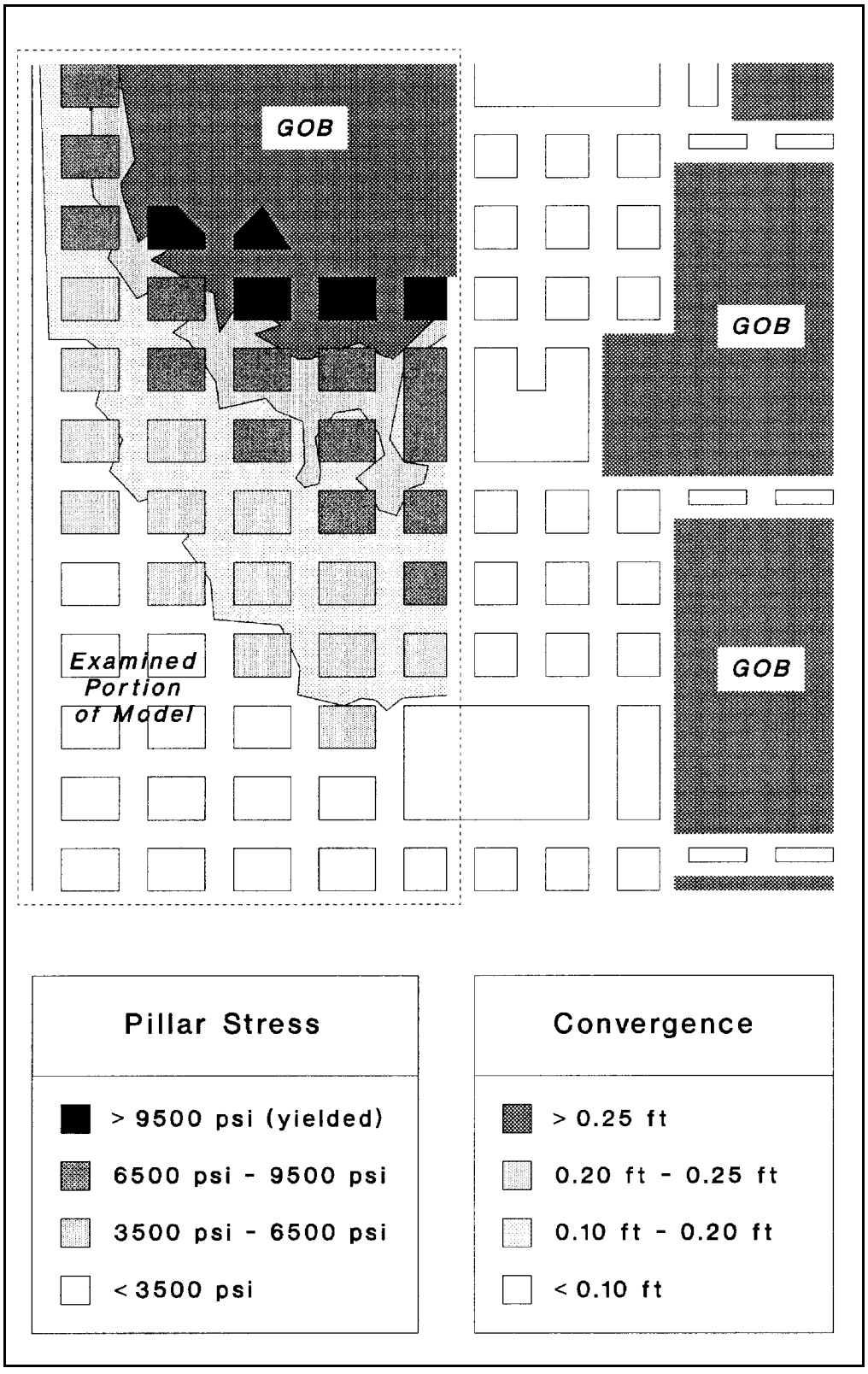

Figure 12.—Case study: BESOL output pillaring section - roof fall area.

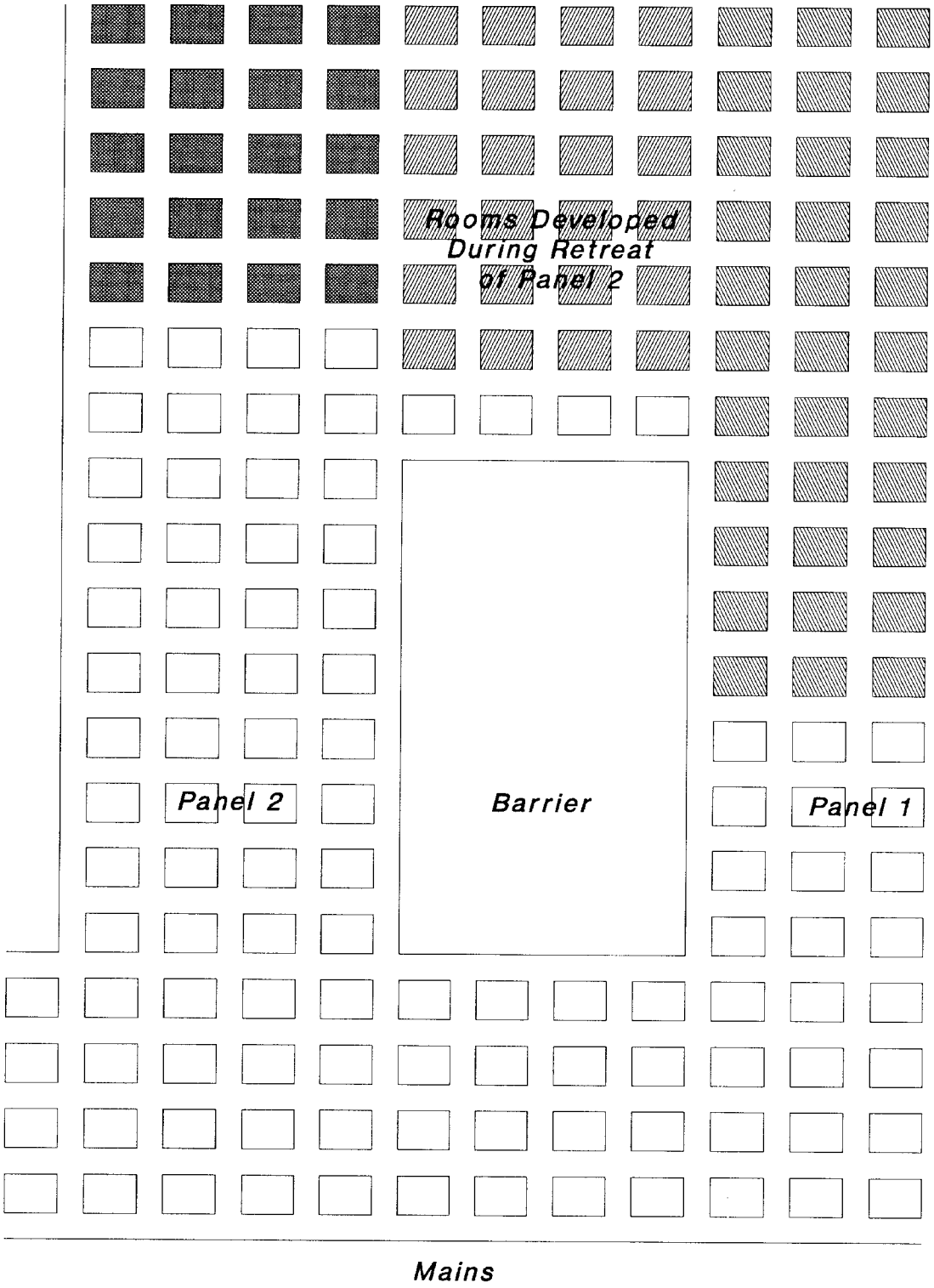

Figure 13.—Case study: full pillaring plan.

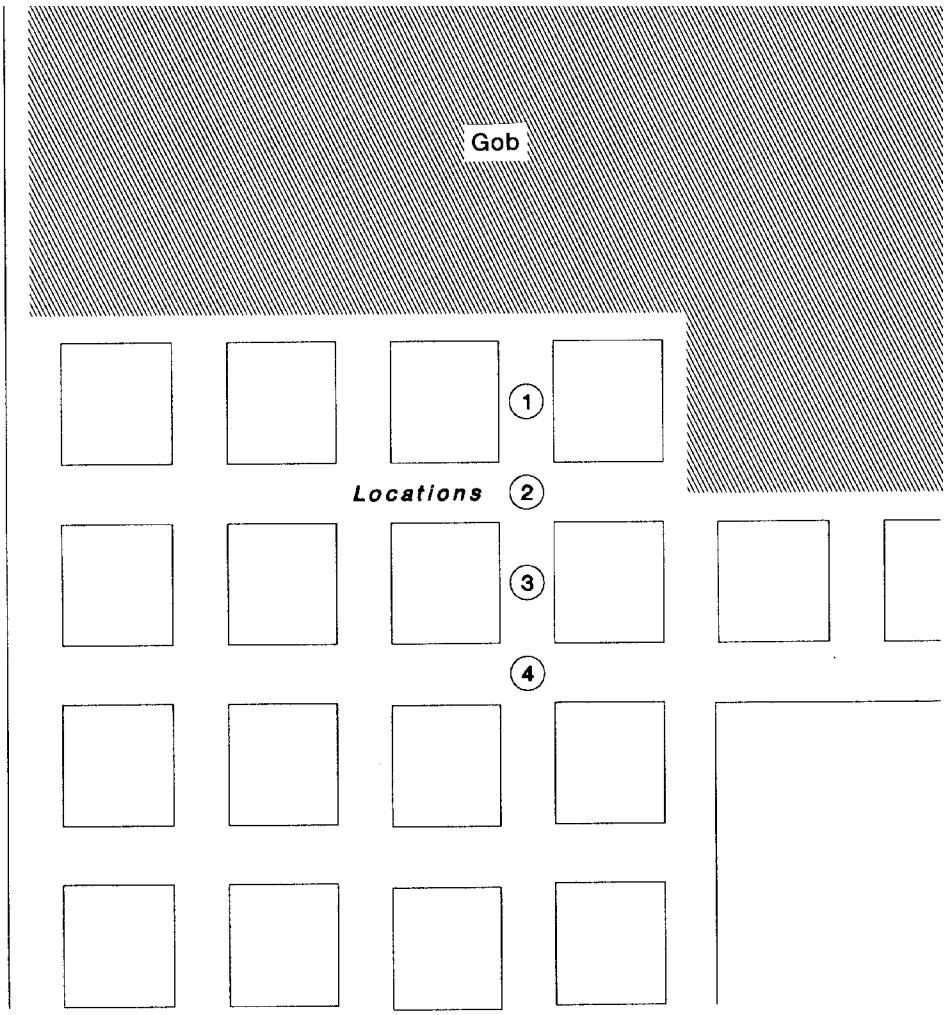

Figure 14.—Case study: full pillaring analysis locations.

but the occurrence of severe conditions should be avoided or at least limited to location 1.

Table 4 presents the BESOL and predicted deterioration index data for each of the four locations for a number of scenarios. The analysis indicated that the use of 40- by 30-ft pillars would result in good conditions through a depth of 400 ft and that 40- by 40-ft pillars would be effective up to 600 ft of cover. Pillars 50- by 50-ft in size would be needed for deeper cover areas, although severe conditions could be possible at locations 1 and 2 as the depth approaches 900 ft.

CONCLUSION

Boundary-element modeling has proven to be an effective tool for mining engineers to resolve complex ground control problems. The techniques set forth in this paper describing coal, rock, and gob behavior have been effectively used to evaluate a variety of mining scenarios. Although they are supported by a number of in situ measurements and have resulted in near duplication of underground conditions in many instances, they provide only a first estimate of parameters that must be validated. Successful numerical simulation requires a substantial effort, including the observation of conditions in many areas and the often repetitive process of calibrating model parameters. The use of techniques such as the deterioration index/regression method has greatly facilitated the linking observed and simulated mine conditions. It cannot be overemphasized, however, that in order to be of any value, a numerical model *must* be validated and provide a realistic representation of the underground environment for which it is applied.

REFERENCES

Bieniawski ZT [1984]. Rock mechanics design in mining and tunneling. A. A. Balkema, 272 pp.

Carr F, Wilson AH [1982]. A new approach to the design of multi-entry developments for retreat longwall mining. In: Proceedings of the Second Conference on Ground Control in Mining. Morgantown, WV: West Virginia University, pp. 1-21.

Choi DS, McCain DL [1980]. Design of longwall systems. Trans Soc Min Eng AIME, Vol. 268, pp. 1761-1764.

Crouch SL, Fairhurst C [1973]. The mechanics of coal mine bumps and the interaction between coal pillars, mine roof, and floor. U.S. Department of the Interior, Bureau of Mines, OFR 53-73, pp. 23-27.

Crouch Research, Inc. [1988]. The BESOL system: boundary element solutions for rock mechanics problems: user's guide, version 2.01. St. Paul, MN: Crouch Research, Inc., pp. 5-19.

Holland CT, Gaddy FL [1964]. The strength of coal in mine pillars. In: Proceedings of the 6th U.S. Symposium on Rock Mechanics. Rolla, MO: University of Missouri, pp. 450-466.

Hsuing SM, Peng SS [1985]. Chain pillar design for U.S. longwall panels. Min Sci and Technol, Vol. 2, pp. 279-305.

Mark C [1990]. Pillar design methods for longwall mining. Pittsburgh, PA: U.S. Department of the Interior, Bureau of Mines, IC 9247.

Mark C, Chase FE [1997]. Analysis of retreat mining pillar stability (ARMPS). In: Proceedings - New Technology for Ground Control in Retreat Mining. Pittsburgh, PA: U.S. Department of Health and Human Services, Public Health Service, Centers for Disease Control and Prevention, National Institute for Occupational Safety and Health, DHHS (NIOSH) Publication No. 97-122, IC 9446, pp. 17-34.

Mark C, Iannacchione AT [1992]. Coal pillar mechanics: theoretical models and field measurements compared. In: Proceedings of the Workshop on Coal Pillar Mechanics and Design. Pittsburgh, PA: U.S. Department of the Interior, Bureau of Mines, IC 9315, pp. 78-93.

Molinda GM, Mark C [1993]. The coal mine roof rating (CMRR): a practical rock mass classification for coal mines. In: Proceedings of the 12th International Conference on Ground Control in Mining. Morgantown, WV: West Virginia University, pp. 92-103.

Obert L, Duvall WI [1967]. Rock mechanics and the design of structures in rock. New York, NY: Wiley, pp. 542-545.

Pappas DM, Mark C [1993]. Load deformation behavior of simulated longwall gob material. In: Proceedings of the 12th International Conference on Ground Control in Mining. Morgantown, WV: West Virginia University, pp. 184-193.

THE FRACTURE MECHANICS APPROACH TO UNDERSTANDING SUPPORTS IN UNDERGROUND COAL MINES

By James M. Kramer, Ph.D.,[1] George J. Karabin, P.E.,[2] and M. Terry Hoch[3]

ABSTRACT

This paper introduces the fracture mechanics approach—a unique way to predict the stability of a coal mine panel. The technique uses analytic equations to calculate the stress, strain, and yield characteristics of coal support systems. It uses fracture mechanics to model almost every type of mine support structure. Another feature is a method that incorporates field-tested knowledge into the analytical analysis. For example, this technique can model the yield characteristics of a coal seam by combining empirical pillar strength equations into the analytic analysis. It may be possible to simulate multiple-seam mining by incorporating subsidence methods into the analysis. The method is simple and quick, which makes it attractive for stress analysis software. It should be more accessible to those in the mining industry who do not have expertise in rock mechanics or numerical modeling. Although the purpose of this research is for modeling coal mines, it should be adaptable to any mine in a tabular deposit.

[1]Mining engineer.
[2]Supervisory civil engineer.
[3]Chief.
Roof Control Division, Pittsburgh Safety and Health Technology Center, Mine Safety and Health Administration, Pittsburgh, PA.

INTRODUCTION

This paper presents a new way to analyze the mechanical behavior of underground coal mine supports. Included are analytic expressions describing the stress, strain, and yielding characteristics of a coal seam. The *fracture mechanics approach* (FMA) provides the capability to model almost every type of mine structure, including pillars, yield pillars, longwall gob, chocks, cribs, posts, and hydrostatic loads. In addition, it predicts pillar stability by combining empirical pillar strength equations into the analytic analysis. This makes the procedure useful for understanding how various support structures affect the mechanical performance of a mine panel.

Although the method is not as sophisticated as numerical analysis, it offers several advantages. The analytic equation makes it is as accurate as numerical modeling, but quicker and easier to use. Because of the few equations involved, it is easy to incorporate the process into a computer spreadsheet or programmable calculator. Real-time design analysis is possible by incorporating the technique into computer code. For example, one can change a design structure (e.g., add a crib) and see instantly the resultant stress effect. The coal yielding process uses empirical pillar strength equations derived from years of field measurements. Combining these equations into the analytic analysis provides insight into pillar stability. The system presented in this paper offers a unique perspective from which to study mine panel stability.

DESIGNING SUPPORT STRUCTURES FOR COAL MINES

There are several ways to analyze the stability of a mine layout. The easiest and, in some cases, most reliable is to use pillar strength equations. These equations are developed from extensive knowledge of coal seam behavior [Mark and Iannacchione 1992]. Most are based on physical stress measurements; however, some come from numerical studies or analytic equations. All of these methods use the pillar width-to-height ratio as the controlling factor. These strength equations can be accurate; however, they assume that the coal pillar is the single means of support. It is not possible to study the effects of cribs, posts, longwall gob, chocks, etc. Also, these equations do not predict the stress distribution through the panel, nor do they predict the extent of the yield zone in the coal.

There are other, more accurate, ways to analyze stability. Numerical modeling, if used properly, can be very accurate. It can predict the stress distribution throughout the entire mine environment, including the coal seam, surrounding strata, slips, faults, and all types of supports. However, this method is time-consuming and requires a certain amount of technical skill. For example, using finite elements, it would take a skilled engineer a day or more to analyze the yield zone in a coal pillar based on data derived from field measurements.

This paper discusses a simple, quick, and accurate solution for predicting the stress distribution in coal pillars and other structures. It uses a combination of fracture mechanics and empirically derived techniques to predict the extent of the yield zone in a coal pillar. It can model nearly every structure used for mine support. Numerical modeling will validate the accuracy of the technique.

THE FRACTURE MECHANICS APPROACH

Understanding the FMA requires visualizing a coal seam as an extremely thin layer in the stratum of the Earth. A tunnel or opening in the coal would appear as a thin crack in an infinite mass.[4] It should then make sense that it is possible to use the mechanics of cracks to analyze the stresses surrounding openings in coal seams.

Visualizing a mine opening as a crack is not new; others applied it to their research [Barenblatt 1962; Hacket 1959; Crouch and Fairhurst 1973; Berry 1960, 1963]. However, this paper describes a way to use the fracture mechanics directly to predict pillar stress. Combined with a superpositioning technique, it is possible to obtain the complete stress distribution throughout the mine panel. A yielding technique completes the analysis by offering realistic characteristics to the coal pillars.

Westergaard's equation is fundamental to fracture mechanics theory and is also the basic equation for the FMA [Westergaard 1939]. The stress distribution at the crack tip is identical to the distribution adjacent to a mine opening. Westergaard describes the stress at the tip of a crack as

$$F_y(x) = \frac{Fx}{\sqrt{x^2 - a^2}}, \qquad (1)$$

[4] In this paper, the term “crack” infers a mine opening and vice versa. Therefore, crack-tip stress is the same as rib or pillar stress.

where $F_y(x)$ ' stress distribution adjacent to a crack tip,

a ' 1/2 the crack width,

F ' in situ stress,

and x ' distance from the center of the crack.

This equation implies that the only parameters needed to predict elastic rib stress are the entry width and the in situ stress (figure 1). Westergaard derived equation 1 by assuming that the stress field acting on the crack is located at an infinite distance from the crack surface. Another assumption is that the crack width must align with the planes of this stress field. In general, these conditions are similar to a mine environment. The Westergaard equation will accurately predict the stress distribution into the coal seam provided that the analysis remains within the elastic range.

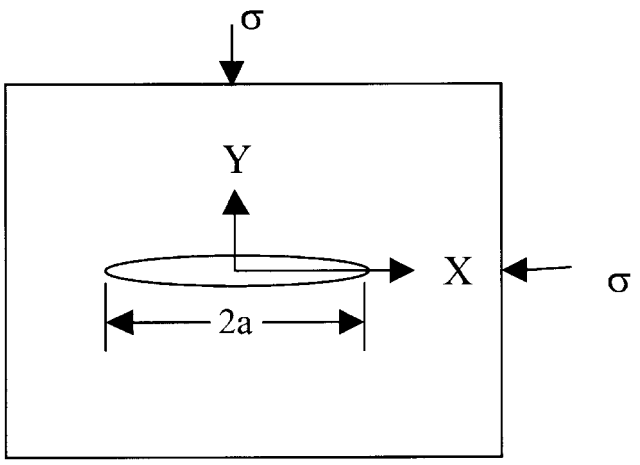

Figure 1.—Crack of width 2a subjected to a uniform biaxial stress field.

NUMERICAL METHODS VALIDATE THE WESTERGAARD EQUATION FOR MINE ANALYSIS

Westergaard developed his stress function by making the following assumptions: the crack has a thickness of zero; it is contained in an infinite, homogeneous plate; and the plate is subjected to a uniform biaxial stress field. These conditions match fairly the conditions encountered in a coal mine opening. There are differences, however. A mine opening has an actual thickness. The structural properties of the coal differ from those of the surrounding rock mass. Also, a coal mine's environment is under the influence of a graduated, nonuniform, biaxial stress field controlled by gravity. It is necessary to consider all of these factors to validate the FMA. Previous research demonstrates the accuracy of the FMA by comparing it to numerical modeling output [Kramer 1996]. It is shown that the technique matches the numerical modeling predictions with a high degree of accuracy.

Figures 2 through 7 are plots that compare the stress prediction of the FMA with that of numerical modeling. The purpose is to show how well the FMA can predict stress even in conditions less ideal than those used by Westergaard to derive equation 1. Such conditions are similar to those encountered in an underground coal mine. All of the evaluations use FLAC[5] as the numerical modeling software. Spreadsheet graphs are used to compare the FMA stress prediction with that determined by FLAC. Each demonstrates that the FMA compares reasonably well with the FLAC model for varying conditions of nonhomogeneity. Initially, the model is homogeneous and simple. The FMA matches extremely well with the numerical model [Kramer 1996]. Then, in order to introduce nonhomogeneity into the numerical model, each individual structural property is altered independently and the results are compared with the FMA. Finally, an evaluation is made between the FMA and a nonhomogeneous numerical model consisting of strata with properties even more variant than an actual mine environment.

Figure 2 charts the comparative stress predictions between the FMA and FLAC for a simple, elastic, and homogeneous model. Note that the stress distributions are nearly exact. The only real difference is at the edge of the mine opening. This difference is due to the approximation technique used in numerical analysis. The model in figure 3 has the same homogeneous properties as those for figure 2; it plots the stress distribution through various planes in the coal seam. This illustrates that the distribution, at any plane, remains consistent with the distribution through the center plane of the seam. Figures 4 and 5 demonstrate that the coal's modulus of elasticity or Poisson's ratio has little effect on the stress distribution through the center plane of the coal seam. The next step is to compare the accuracy of the FMA for predicting the stress of a nonhomogeneous numerical model. Figures 6 and 7 relate the results of the simulation.

Figure 6 shows the comparison between FLAC and the FMA for the stress distribution produced in a graduated, nonuniform, biaxial stress field similar to that encountered in an underground mine. For these studies, the horizontal stress is 0.3 times the vertical stress. The design of the model places the coal seam at a depth of 381 m. The structural parameters of the coal and rock are equivalent. This study also compares the Westergaard equation to the stress at various planes in the seam (figure 6).

It can be seen that the nonuniform stress field in the numerical model causes a deviation in stress from the Westergaard prediction; however, most of the difference is near the edge of the mine opening. In this portion of the mine rib, the coal is yielding. Analytical methods do not exist for predicting the stress distribution in this region. Introduced later in this paperis a method that uses field measurements to describe the stress distribution in the yield zone of a coal rib.

[5] Fast Langrangian Analysis of Continuum, Itasca Corp., Minneapolis, MN.

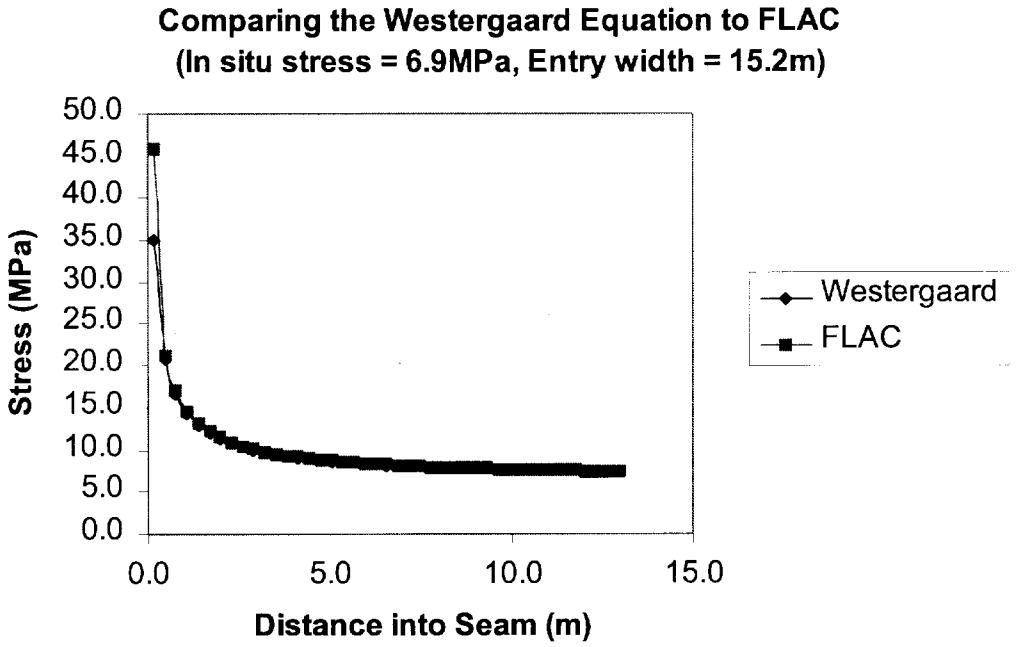

Figure 2.—Stress distribution in a coal seam next to a mine opening: comparison between numerical analysis and the Westergaard equation. Homogeneous model.

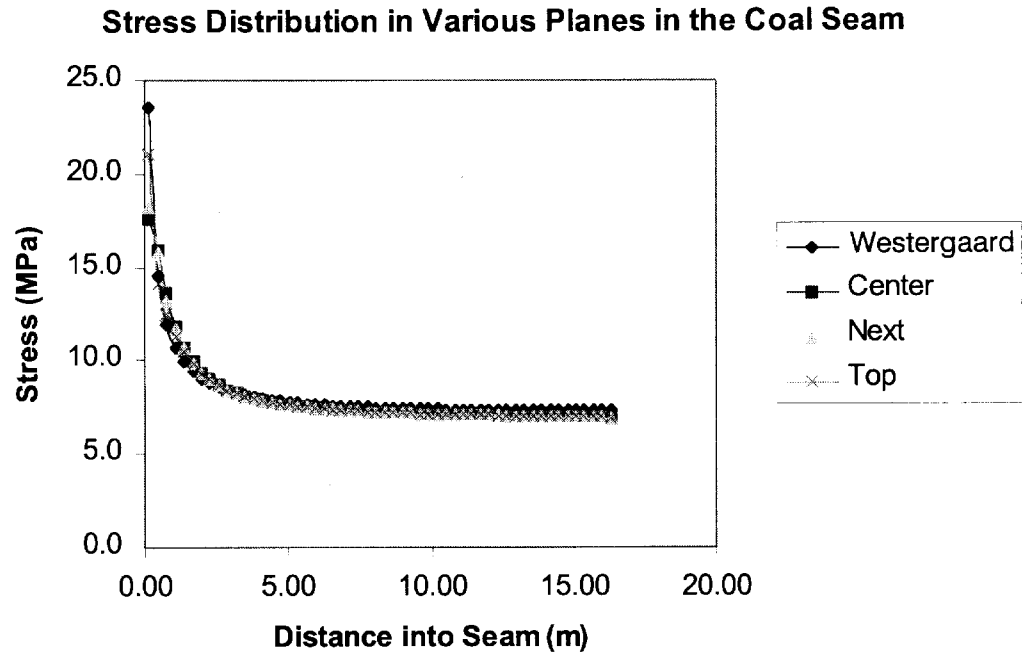

Figure 3.—Stress distribution at various levels in the coal seam. Properties similar to the model in figure 2.

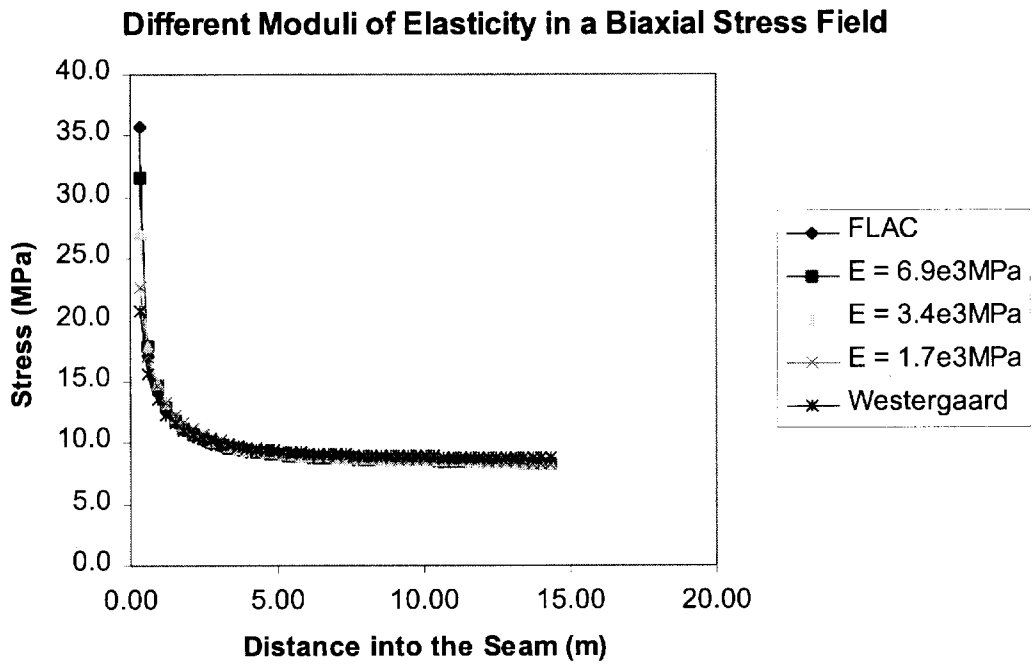

Figure 4.—Stress profile for coal with different moduli. Four separate FLAC models.

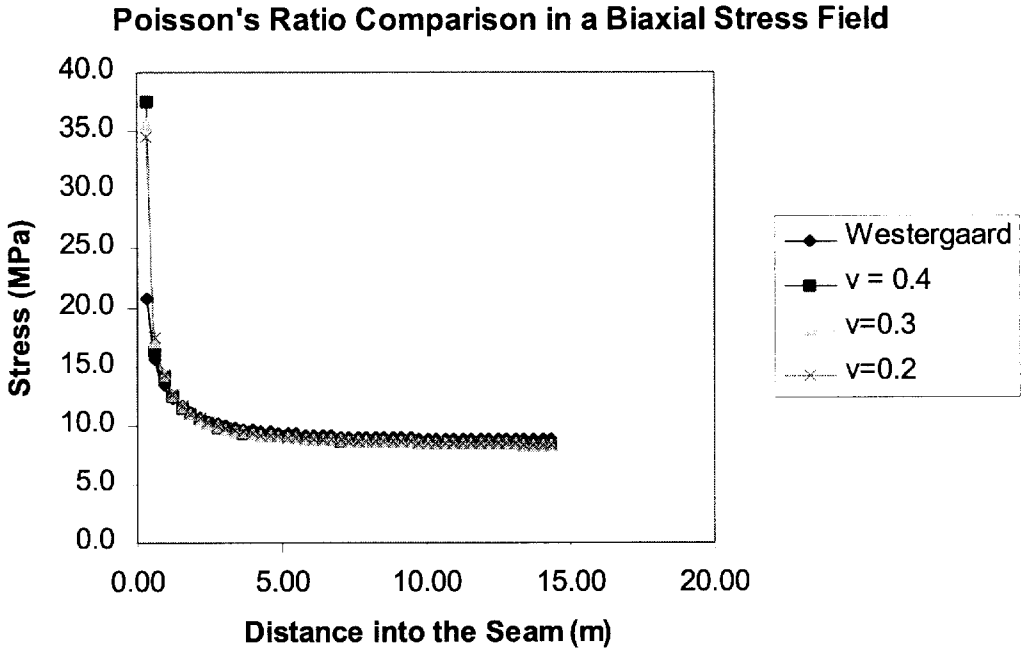

Figure 5.—How the Poisson ratio affects the stress distribution. Three separate FLAC models.

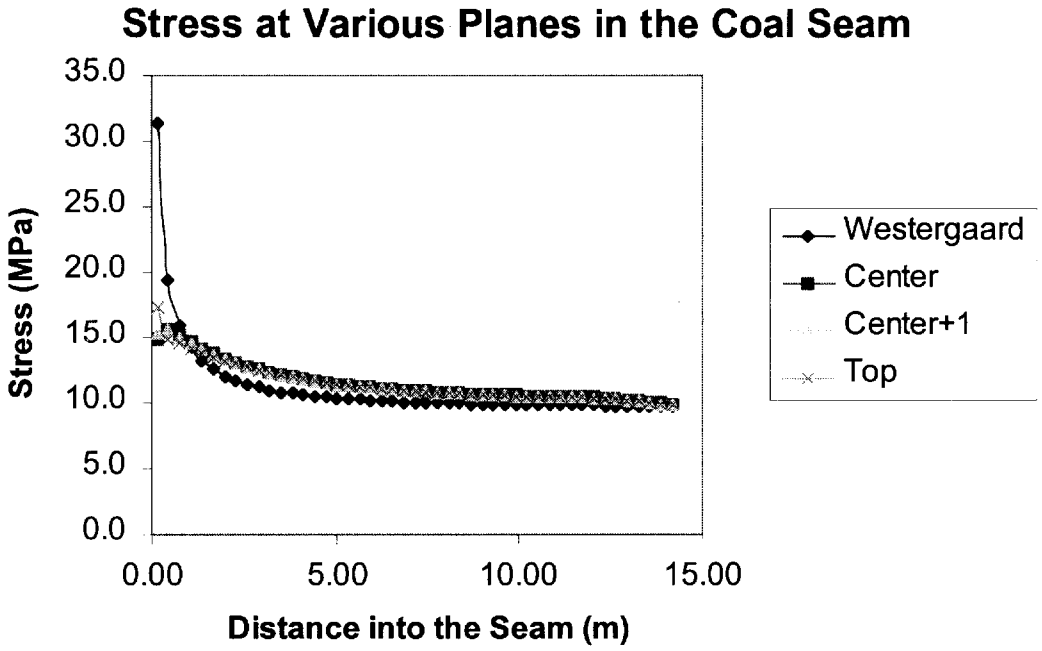

Figure 6.—The effect of a graduated, nonuniform biaxial stress distribution similar to conditions underground. Stress profile at various levels in the seam.

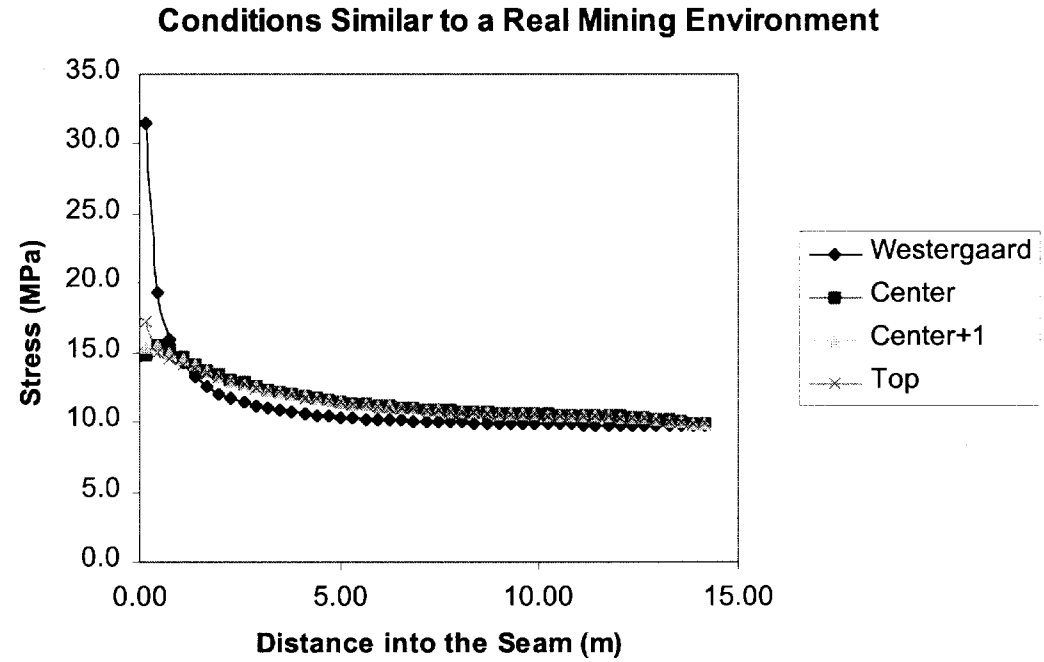

Figure 7.—Comparison of a model simulation of a real mine environment.

The numerical model described below will validate the FMA's ability to analyze structural variations found in a real mine environment. In this model, the strata are nonhomogenous. In addition, the surrounding stress field is variable in both the vertical and horizontal planes. Such a model has structural variations greater than those encountered in most coal mines. The surrounding rock mass has a Young's modulus of 27,580 MPa and a Poisson's ratio of 0.2. The unit weight of this mass is 0.03 MN/m^3. The coal seam has a Young's modulus of 3,448 MPa, a Poisson's ratio of 0.3, and a unit weight of 0.03 MN/m^3. The unit weights are high to enhance the stress comparisons by increasing the effect of gravity loading. To show the effect of mining in an area subjected to a high stress field, the model is initialized with a premining stress prior to adding the mine opening. Adding a mine opening to a model with a high biaxial stress field already in place would alter the stress in the areas adjacent to the mine opening. Figure 7 compares the Westergaard equation to FLAC's analysis for different levels in the coal seam. The distributions vary considerably; however, most of this deviation is near the mine opening. In this area, the coal will yield. A technique will be presented in this paper that describes the stress distribution in the yield zone of the coal.

THE POINT-FORCE METHOD USED TO SIMULATE MINE SUPPORTS

An essential concept of the FMA is the process by which a point force, acting on the surface of the crack, affects the stress intensity at the crack tip. In mining, this point force could be a mine post or hydraulic jack. A continuous series of point forces can model a yield pillar, longwall gob, the yield zone of the pillar, or any other type of mining supports [Kramer 1996]. Figure 8 depicts a crack with an internal point force, P, pushing out against the crack surface. This force P is at a distance x from the crack center. This force affects the stress intensity factor K at points A and B. The point force is similar to the loading from a single-point mine support, such as a post or hydraulic jack.[6]

Green functions are used to predict the stress intensity factors [Paris and Sih 1965]. The factors are:

$$K_A = \frac{P}{\sqrt{Ba}} \sqrt{\frac{a+x}{a-x}} \qquad (2)$$

$$K_B = \frac{P}{\sqrt{Ba}} \sqrt{\frac{a-x}{a+x}} \qquad (3)$$

where K_A = stress intensity at point A,

K_B = stress intensity at point B,

P = point force,

a = 1/2 the opening width,

and x = distance from opening center

[6]The stress intensity factor is of utmost importance in the study of fracture mechanics. It is a measure for the stress singularity at the crack tip. For the case of uniaxial compression with force P at infinity, K must be proportional to P. K_A and K_B must also be proportional to the square root of a length. For an infinite object, the only characteristic length is the crack size; thus, K must take the form: $K = F/(Ba)$.

YIELD PILLARS

Yield pillars are common in longwall mining; they control floor heave and/or fine tune roof behavior. As the name implies, the pillars yield, thus redistributing the load around a control area in the mine. It is possible to model yield pillars as a continuous series of point forces. Equations derived from in situ pillar strength measurements can determine the intensities of the point forces. However, for the present discussion, the point forces are considered uniform and equal to the yield strength of the coal (figure 9).

To illustrate the method, it is necessary to discuss only the stress effect at a single crack tip (e.g., point A in figure 9). Either equation 2 or equation 3 can describe the stress intensity at point A. The correct equation to use depends on the location of the point forces with respect to the a-origin. In the discussion below, the location of the point forces (figure 9) is chosen to provide the most complete example of the technique. Because the locations of the point forces are equally distributed on both sides of the origin, solution to the stress effect at point A requires using a combination of equations 2 and 3. In

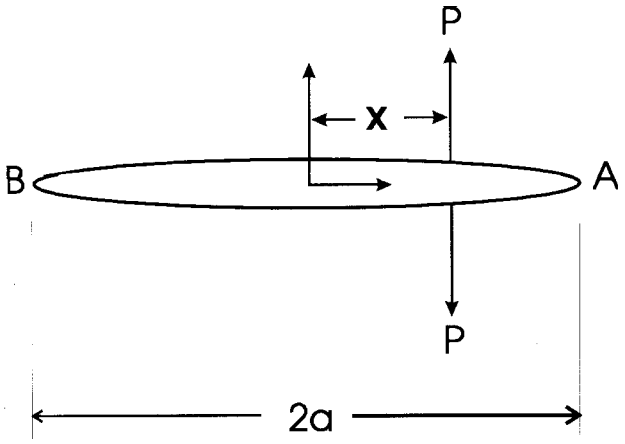

Figure 8.—Crack with wedge forces at x.

absence of the yield pillar, the stress intensity at point A is [Dugdale 1960]:

$$K_{insitu} = F_{insitu}\sqrt{Ba}\,. \tag{4}$$

The yield pillar will act to reduce this intensity. The a-origin is located in the center of the point forces; thus, the distribution in the &x side is equal to the distribution in the %x side (figure 9). The stress intensity factor at point A caused by the continuous point forces on the %x side of the origin is

$$K_{\%x} = K_A = \frac{F_{ys}}{\sqrt{Ba}} \int_0^d \sqrt{\frac{a\%x}{a\&x}}\,dx\,. \tag{5}$$

The stress intensity factor at point A caused by the continuous point forces on the &x side of the origin is

$$K_{\&x} = K_A = \frac{F_{ys}}{\sqrt{Ba}} \int_0^d \sqrt{\frac{a\&x}{a\%x}}\,dx\,. \tag{6}$$

The stress intensity factor for the yield pillar becomes

$$K_{yield} = K_{\%x} \% K_{\&x}. \tag{7}$$

With the yield pillar in place, the stress intensity factor at point A becomes

$$K_{total} = K_{insitu} \& K_{yield}. \tag{8}$$

The Westergaard equation relates rib stress to the in situ stress and the width of the opening. Because K_{total} includes not only the in situ stress but also the effect of the yield pillar, it is necessary to modify the Westergaard equation to reflect this effect. It is necessary to modify the Westergaard equation by substituting a dummy variable in place of a real variable. The opening half-width variable "a" is the proper choice for the substitution.[7] Solving for "a" in K_{total} and substituting it into the Westergaard equation as a dummy variable will provide the proper stress distribution at point A. The following demonstrates the concept.

The stress intensity factor is defined as

$$K = F\sqrt{Ba}\,. \tag{9}$$

To modify the Westergaard equation, it is necessary to substitute values and solve for the unreal "a", making it a dummy variable such that

$$a_{dummy} = \frac{K_{total}^2}{BF_{insitu}^2}\,. \tag{10}$$

The reduced Westergaard stress distribution at point A then becomes

$$F_{modified}(x) = \frac{F_{insitu}\,x}{\sqrt{x^2 \& a_{dummy}^2}}\,. \tag{11}$$

[7]Modifying F would result in the stress distribution leveling to a value below the in situ stress.

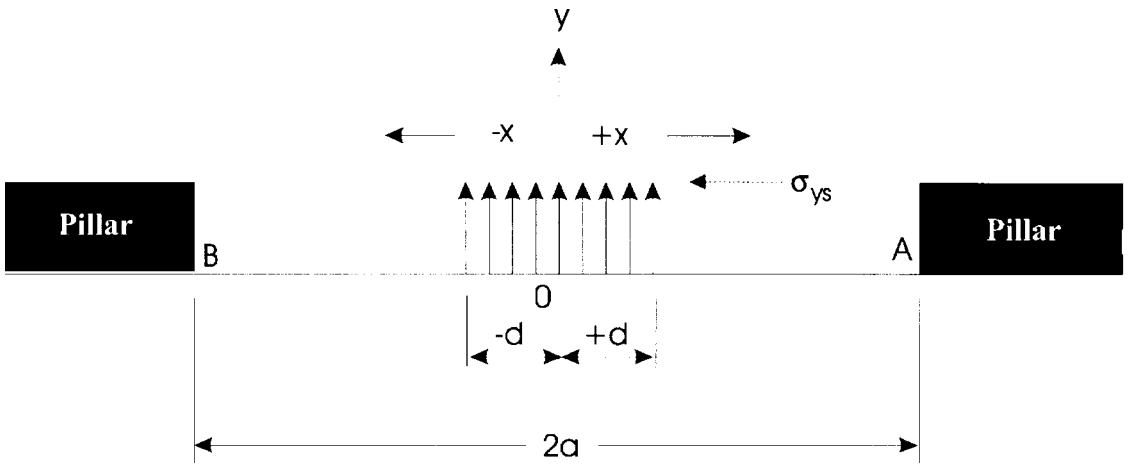

Figure 9.—Yielded pillar modeled as a continuous set of point forces.

LONGWALL GOB

The technique used to model longwall gob is similar to that for the yield pillar. An assumption can be made that the center of the gob is in contact with the roof and floor and the material is compacted completely. Due to symmetry, it is necessary to model only one-half the gob width to determine its effect on the stress intensity at the tip of the opening. Therefore, the opening extends from the gob center to edge of the gate pillar at point A (figure 10). The residual strength of this material is a function of the amount of compaction. Because the center of the gob has the greatest compaction, it has the greatest residual strength; the outside edge of the gob has the least. To simulate gob material, the point forces are high in the center of the gob and low at the edge. Originally, the following example was formulated using U.S. customary units of measurement. Conversion to the metric system makes some values appear awkward.

As usual, the a-origin and x-origin begin at a point equidistant from point A and the gob center. The point forces to the right of the origin (i.e., %x side) would use equation 5 to analyze the effect at point A; the point forces to the &x side of the origin will use equation 6. "Derive—A Mathematical Assistant"[8] is used to solve for the integral in each equation. Included in table 1 are the input variables and resultant stress intensity factors for the gob depicted in figure 10. The gob material in the model is divided into six sections, each reflecting a different yield strength (YS_1 to YS_6). The first three sections are in the &x side (K_B side) of the origin; the other three are in the %x side (K_A side). The location of the section determines which point-force equation to use. The total effect of the gob is the summation of the K-values for all six sections:

$$K_{gob} = K_1 + K_2 + K_3 + K_4 + K_5 + K_6. \qquad (12)$$

This value is subtracted from the K_{insitu} value (the stress intensity for the large opening without the gob material in place) to obtain the proper stress intensity factor at point A. The relation is

$$K_{total} = K_{insitu} - K_{gob}. \qquad (13)$$

EXAMPLE

Below is an example that demonstrates the technique. It analyzes the effect from two sections of the complete model shown in figure 10. These particular sections (sections 3 and 4) were chosen to illustrate forces on either side of the axis origin. The point forces in section 3 align in the &x direction; those in section 4 are in the %x direction. The stress intensity factor will be determined using a combination of equations 5 and 6. Table 1 lists the results from the complete analysis.

[8]Derive—A Mathematical Assistant," Soft Warehouse, Inc., 3660 Waialae Ave., Honolulu, HI.

Input Parameters:

Width of longwall face = 232 m
1/2 width of longwall face = 116 m
2a (width of longwall face plus gate entry) = 122 m
a = 61 m
F_{insitu} = 13.8 MPa

Section 3:

The yield strength for section 3 is F_{ys3} = 12.4 MPa. It occupies the &x portion of the a-axis for the 0- to (&)18.3-m segment. The effect on the stress intensity at point A due to section 3 of the gob is

$$K_3 = \frac{F_{ys}}{\sqrt{Ba}} \int_0^{18.3} \sqrt{\frac{a - x}{a + x}}\, dx$$

$$= \frac{12.4}{\sqrt{B61}} \int_0^{18.3} \sqrt{\frac{61 - x}{61 + x}}\, dx$$

$$= 14.1$$

NOTE: Although the point forces are in the -x region, the limits of the integral are from 0 to (%)18.3 m.

Section 4:

The yield strength for section 4 is F_{ys4} = 10.3 MPa. This section occupies the %x portion of the a-axis for the 0- to (%)18.3-m segment. The effect on the stress intensity at point A due to section 4 of the gob is

$$K_4 = \frac{F_{ys}}{\sqrt{Ba}} \int_0^{18.3} \sqrt{\frac{a + x}{a - x}}\, dx$$

$$= \frac{10.3}{\sqrt{B61}} \int_0^{18.3} \sqrt{\frac{61 + x}{61 - x}}\, dx$$

$$= 15.9$$

"Derive—A Mathematical Assistant" solved both of these integrals. The solutions yield a rather cumbersome equation that is impractical to include in this paper; however, it can be incorporated into spreadsheet software or computer code. Table 1 includes the K factors for all six sections of the longwall gob. The effect on the stress intensity factor at point A caused by all six sections is

$$K_{gob} = K_1 + K_2 + K_3 + K_4 + K_5 + K_6$$
$$K_{gob} = 13.8 + 10.7 + 14.1 + 15.9 + 18.0 + 25.8$$
$$K_{gob} = 98.3$$

Table 1.—Input variables and stress intensity factors for each section of the longwall panel depicted in figure 10

	Section 1	Section 2	Section 3	Section 4	Section 5	Section 6
F_{ys}, MPa	13.8	13.1	12.4	10.3	8.3	6.9
x-range, m	61.0-36.6	36.6-18.3	18.3-0	0-18.3	18.3-36.6	36.6-55.0
Stress intensity at point A (%x side)	—	—	—	15.9	18.0	25.8
Stress intensity at point A (&x side)	13.8	10.7	14.1	—	—	—
K_{gob}	98.3	—	—	—	—	—

Input parameters:
Width of longwall face ' 232 m
1/2 width of longwall face ' 116 m
2a (width of longwall face plus gate entry) ' 122 m
a ' 61 m
F_{insitu} ' 13.8 MPa

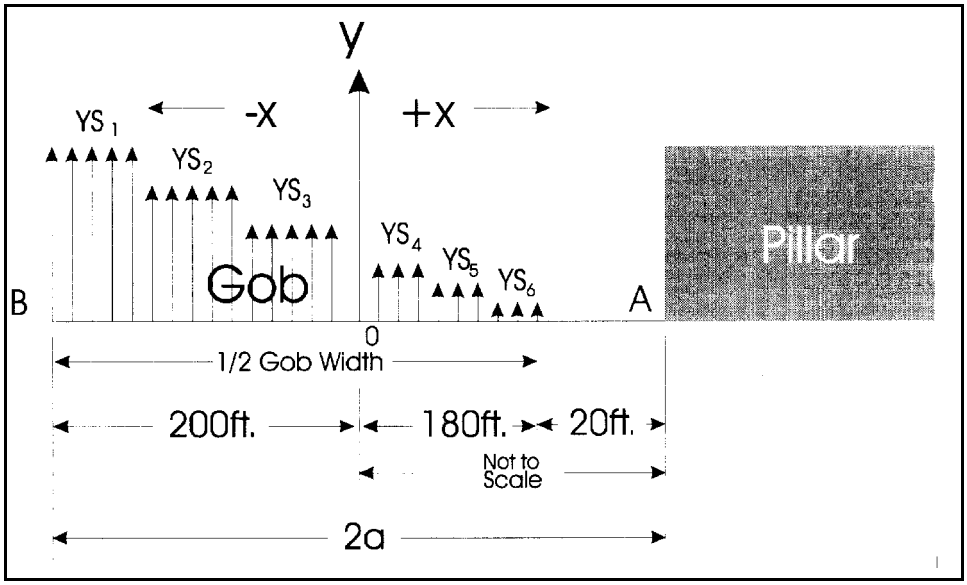

Figure 10.—Longwall gob simulated as point forces of different strengths.

Equation 4 determines the stress in absence of the gob (point forces) as

$$K_{insitu} = F_{insitu}\sqrt{Ba}$$

$$K_{insitu} = 13.8\sqrt{B61}$$

$$K_{insitu} = 191.0$$

It is necessary to reduce this intensity to reflect the addition of the gob material. The stress intensity factor at point A now becomes

$$K_{total} = K_{insitu} \& K_{gob}$$
$$K_{total} = 92.7$$

The dummy variable used to relate this stress reduction to the Westergaard equation is

$$a_{dummy} = \frac{K_{total}^2}{BF_{insitu}^2}$$

$$a_{dummy} = \frac{(92.7)^2}{B(13.8)^2}$$

$$a_{dummy} = 14.4 \text{ m}$$

The modified Westergaard distribution at point A becomes

$$F_{modified}(x) = \frac{F_{insitu}x}{\sqrt{x^2 \& a_{dummy}^2}}$$

$$F_{modified}(x) = \frac{13.8x}{\sqrt{x^2 \& 14.4^2}}$$

This is the general technique used to model longwall gob. Luo significantly improved the above technique and developed a computer program to model the stability of longwall chain pillars [Kramer et al. 1998].

HYDROSTATIC FORCES

It is possible to measure the effect of hydrostatic forces on the coal seam. A hydrostatic force acts with equal strength in all three cardinal directions. It is similar to the pressure exerted from water or gas. To simulate a hydrostatic force, it is necessary to fill the entire mine opening with a continuous distribution of point forces (figure 11). In order to test the hydrostatic effect, the point forces are set equal to the in situ stress (13.8 MPa). This situation should have the effect of flattening the stress distribution at point A to a level equal to the in situ stress.

Figure 12 is a plot of the stress distribution. It can be seen the distribution is almost uniform and equivalent to the in situ stress. This further demonstrates that the point-force method accurately describes the effective stress distribution at the mine rib.

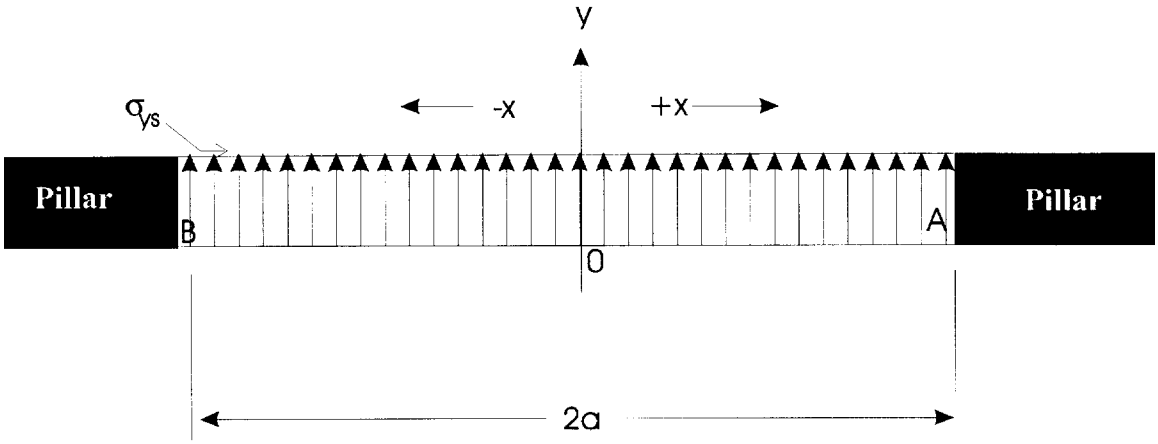

Figure 11.—Crack opening completely filled with point forces equal to the in situ stress.

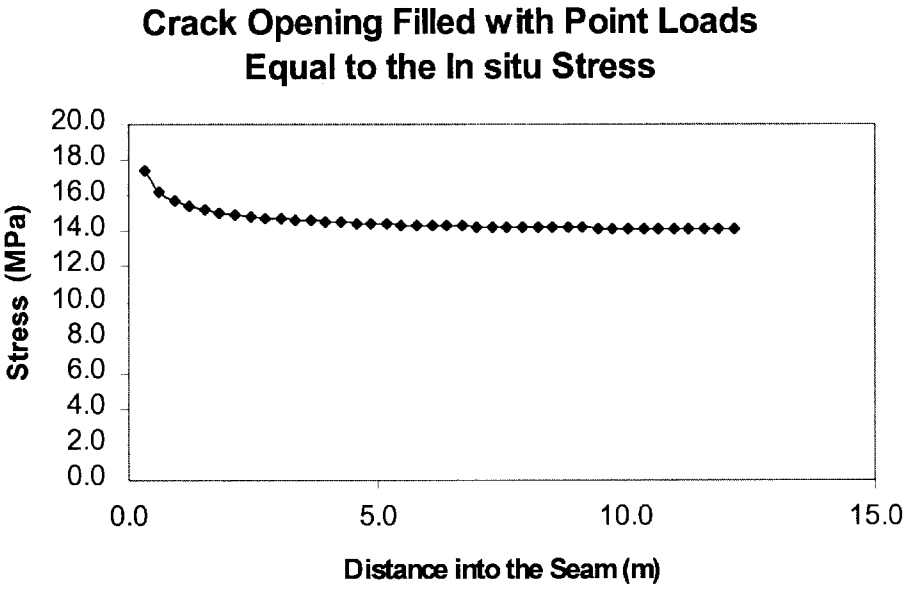

Figure 12.—Stress distribution at point A is nearly flat and equal to the in situ stress.

TECHNIQUE TO COMBINE DIFFERENT MINE SUPPORTS

It is possible to combine any type of mine supports and predict the resultant stress distribution in the coal seam. Figure 13 presents a typical mining environment combining the following structures: a longwall gob, a yield pillar, and a crib. Analyzing this arrangement requires a combination of the stress intensity factors for each support member. This combined value is used to reduce the total stress intensity at point A. The procedure for doing this is as follows:

- Calculate K_{insitu} for point A
- Calculate K_{gob} for point A
- Calculate K_{yield} for point A
- Calculate K_{crib} for point A
- Combine the stress intensity factors for each support, and use this value to reduce the stress intensity associated with the entire opening width:

$$K_{total} = K_{insitu} + K_{gob} + K_{yield} + K_{crib}$$

EVALUATING PILLAR YIELD

Because coal mines are often located at a great depth below the surface, the stress levels often exceed the yield strength of the coal. It is necessary to account for yielding in the coal pillars to correctly assess structural stability. Fracture mechanics is useful in predicting the yielding characteristics of the coal.

The Westergaard equation introduces a singularity at the pillar edge. This is where the stress distribution approaches infinity. The pillar edge yields and redistributes the loading in order to eliminate the singularity. The yielded zone continues to offer residual support to the roof and floor.

Dugdale provides a way to estimate the length of this yield zone in the pillar [Dugdale 1960; Broek 1982]. The following sections describe how to determine the extent of the yield zone. Also described is a way to predict the stress distribution in the elastic core of the pillar. First, the basic technique used by Dugdale to arrive at his yield zone prediction is reviewed. Later, a technique is introduced that determines the extent of the yield zone specifically in coal.

THE EFFECT OF POINT LOADING ON THE STRESS INTENSITY AT THE CRACK TIPS

As mentioned previously, figure 8 depicts a crack with an internal wedge force P pushing out against the crack surface. This force P is at a distance x from the crack center. These wedge forces affect the stress intensity function, K, at points A and B. It is possible to use equations 2 and 3 to predict these stress intensity factors, K [Paris and Sih 1965]. A form of these equations is fundamental in the development of residual forces supporting the roof and floor in the yielded portion of the pillar.

DUGDALE'S APPROACH TO CRACK TIP YIELDING

Although the pillar edge yields, it has a residual strength that supports the roof and floor of the coal seam. Imagine this residual support as a continuous distribution of dislocated point forces (figure 14). Dugdale determined the extent of the yielded zone by first assuming that the residual strength of each point force is equal to the yield strength, F_{ys}, of a material (in this case, coal) [Dugdale 1960; Broek 1982]. Because the yielded edge is significantly weaker, it would seem as though the mine opening becomes wider. The mine opening would theoretically extend into the pillar to the point where yielding stops. At this point, the singularity disappears because of the canceling effect of the residual stress in the yield zone. The effective mine width, $a_{eff} = a + D$, represents the distance to the new elastic crack tip, where D symbolizes the extent of the yielded zone.

The yielded zone, D, exerts a residual stress equal to the yield stress, $F_{ys.}$ The yield zone, D, depicted as additional opening width, is not really an opening; the material can still bear the yield stress. The size of D is chosen so that the stress singularity disappears: K_{total} approaches zero. This means that the stress intensity, K_{insitu}, due to the uniform in situ stress, F, has to be compensated by the stress intensity, K_D, due to the residual wedge forces F_{ys} [Broek 1982]. In other words:

$$K_{insitu} = -K_D \tag{14}$$

Satisfying equation 14 leads to the determination of D in the following manner. Equations 2 and 3 describe how a point load affects the stress intensity factor, K. If the wedge forces are distributed from s to the effective crack tip, the stress intensity becomes

$$K = \frac{P}{\sqrt{Ba}} \int_s^a \left(\sqrt{\frac{a+x}{a-x}} + \sqrt{\frac{a-x}{a+x}} \right) dx . \tag{15}$$

Solution to this integral is

$$K = 2P\sqrt{\frac{a}{B}} \cos^{-1}\frac{s}{a} . \tag{16}$$

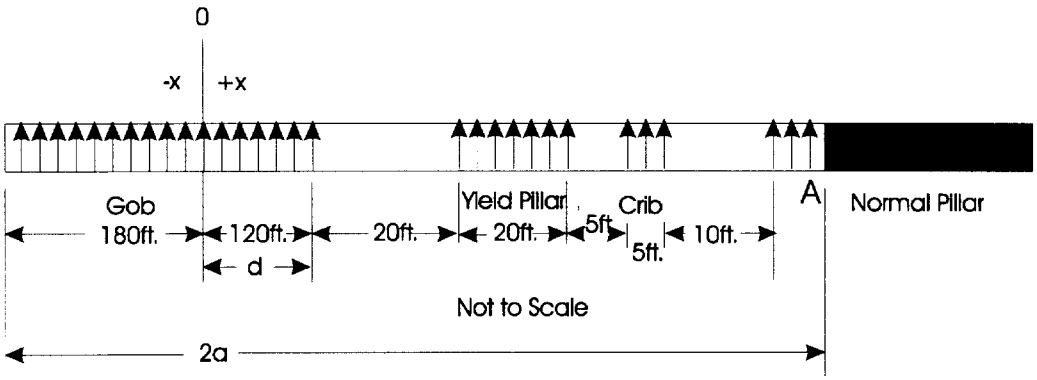

Figure 13.—Modeling various support structures using the point-force technique.

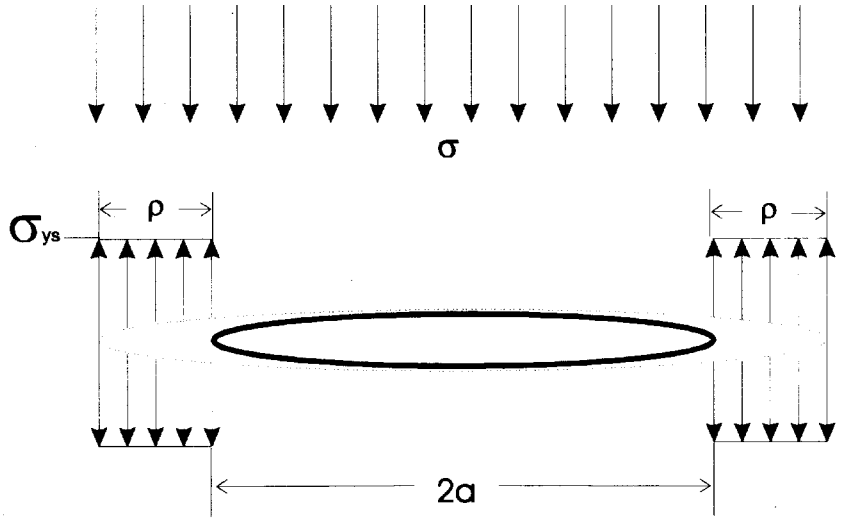

Figure 14.—Continuous point forces approximate the residual pillar strength in yielded zone preceding the elastic crack tip.

Applying this result to the crack in figure 14, the integral has to be taken from s ' a to a ' a % D. Thus, "a" has to be substituted for "s" and "a % D" for "a" in equation 16, while P equals the yield strength, F_{ys} [Broek 1982]. This leads to the determination of the yield zone as

$$D ' \frac{B^2F^2a}{8F_{ys}^2}, \qquad (17)$$

where D is the extent of the pillar yield zone.

Dugdale's description of the yield zone does not provide a simple way to predict the stress distribution in the elastic core adjacent the yielded edge. Irwin presents a method to predict the stress distribution in the elastic portion of the pillar [Broek 1982]. Irwin describes a yield zone that is similar in length to Dugdale's prediction; however, the crack tip extends only one-half the distance (figure 15).

The singularity vanishes if area A ' area B. It was possible to verify this using spreadsheet software. It is particularly accurate for values of F/F_{ys} less than 0.75. Irwin's description produces the stress distribution shown in figure 16. This distribution is not representative with in situ measurements taken at underground mines [Mark and Iannacchione 1992].

PLAIN STRAIN

Dugdale's method concerns conditions of plane stress. Pillar analysis requires a plane strain condition. Studies indicate that for the case of plain strain, the effective yield stress can be as great as three times that for a similar plain stress analysis. This is due to confinement, which increases the triaxial yield strength. Broek suggests modifying the yield stress with the constraint factor:

$$\text{p.c.f.} ' 1.68F_{ys} \qquad (18)$$

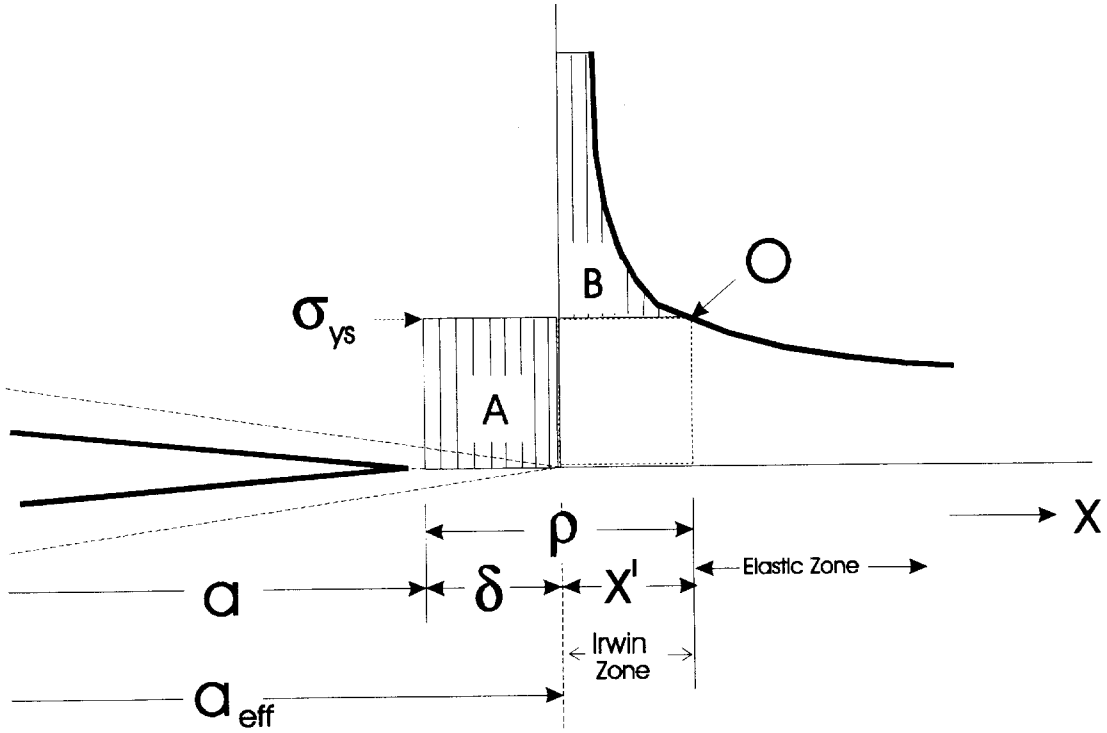

Figure 15.—The Westergaard distribution originates at the beginning of the Irwin zone, but does not take effect until the beginning of the elastic zone.

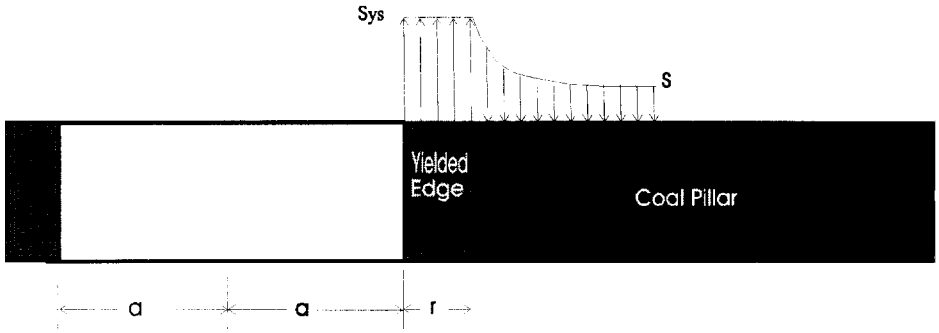

Figure 16.—Pillar stress distribution as predicted by the Dugdale-Irwin method.

THE DUGDALE-IRWIN METHOD AS IT RELATES TO A MINE ENVIRONMENT

Previous research indicates that confinement increases the yield strength of a pillar core [Crouch and Fairhurst 1973; Karabin and Evanto 1999; Sih 1966; Salamon and Munro 1967]. However, the measured pillar stress distribution does not resemble the distribution predicted by Dugdale-Irwin shown in figure 16. Underground measurements show the residual strength should be low at the wall of the mine opening, but increase proportionally with the distance into the pillar core.

The mathematical model predicted by Dugdale-Irwin is accurate; only the visual perception is misleading. The residual stress distribution in the yielded area can take on any shape as long as area A equals area B (figure 17). A more realistic stress distribution such as that in figure 18 should then be possible.

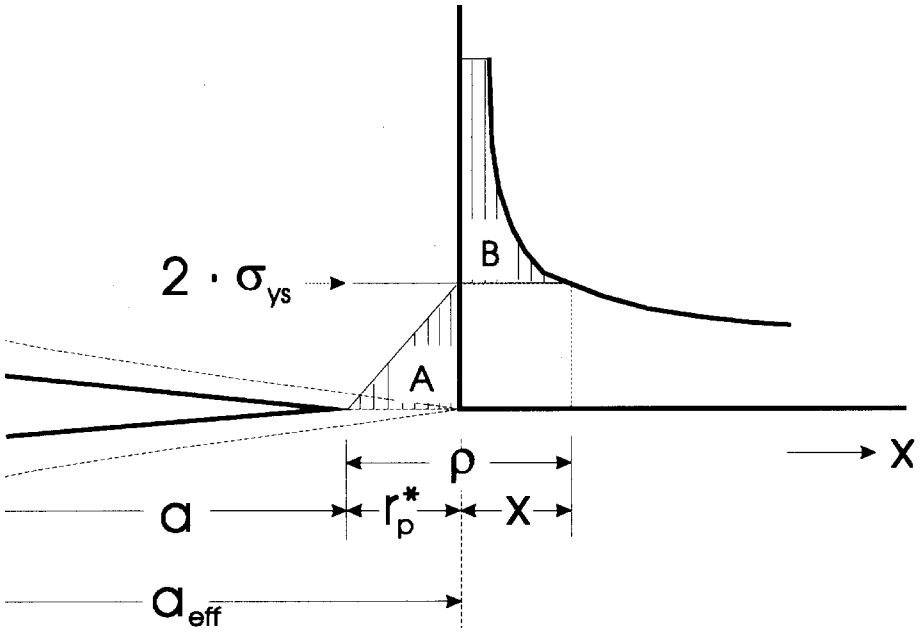

Figure 17.—Yield stress can assume any shape provided that area A equals area B.

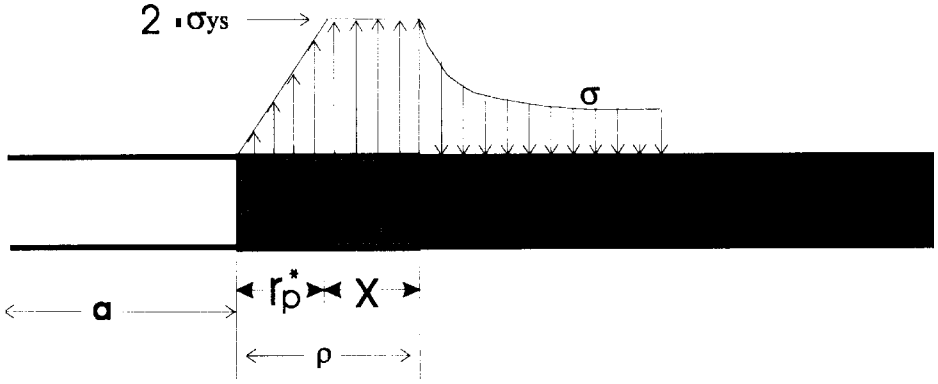

Figure 18.—Possible contour of pillar stress using the Dugdale-Irwin method.

COMBINING EMPIRICAL METHODS INTO THE ANALYTIC ANALYSIS

The Westergaard equation introduces a singularity at the pillar edge; this is where the stress approaches infinity. To eliminate this singularity, the edge must yield and redistribute the load. The yielded edge retains a residual strength that offers confinement to the core.

In situ field measurements demonstrate a nonlinear residual stress distribution in the yield zone of a coal pillar. The stress is low at the pillar rib and increases rapidly into the center of the pillar. This indicates that confinement makes the pillar strength higher than the unconfined compressive strength used by Dugdale-Irwin. It is possible to use the point-force method to model this residual strength and thus predict the extent of the yield zone. It is a common numerical technique to study the yielding coal with a strain-softening model [Crouch and Fairhurst 1973; Wilson 1972]. Figure 19 depicts a model in terms of stress versus strain in a timeframe denoted by peak and post (residual) stress.

It is possible to use any of the popular pillar strength equations to predict the strain-softening characteristics of the coal. The equations of Bieniawski and Holland-Gaddy are the most accepted of these equations [Mark and Iannacchione 1992]. Mark and Iannacchione developed an equation that represents an average of these two equations. It predicts the pillar strength as a function of distance from the opening. This equation is:

$$F_v(x) = S_1 \times \left(0.78 + 1.74 \frac{x}{h} \right), \qquad (19)$$

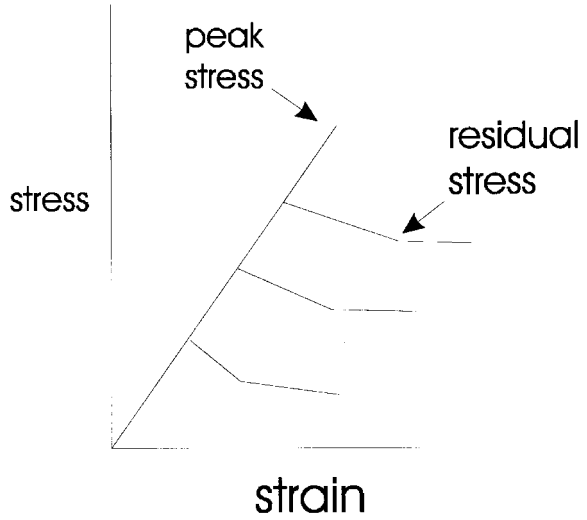

Figure 19.—The stress-strain characteristics in the yield zone of a coal seam.

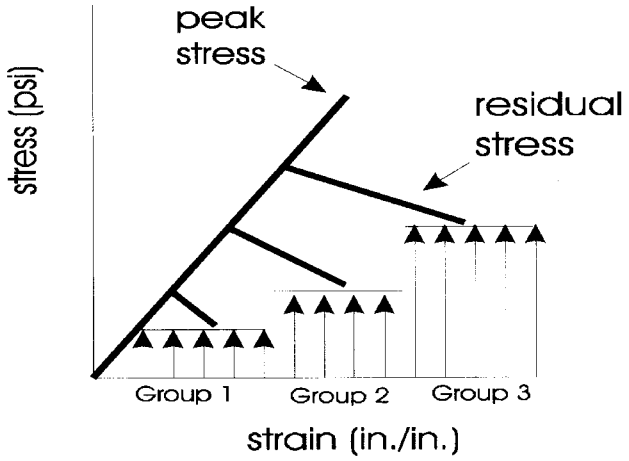

Figure 20.—It is possible to model peak or post stress as several groups of point forces.

where F_v = peak stress at distance x, MPa,

S_1 = in situ coal strength, MPa,

x = distance to the free face, m,

and h = seam height, m.

It is possible to model the stress distribution in the yield zone as a series of point forces (figure 20). These continuous series of point forces has a uniform intensity within each group. Equation 19 will predict the average strength assigned to each group. It is necessary to use an iterative technique to determine the extent of the yield zone. This iterative technique progressively yields each group while testing for the disappearance of the singularity. When $K_p \geq K_{insitu}$, the yielding stops. Luo has eliminated the need for an iterative technique by providing the exact solution for the equation [Kramer et al. 1998].

EXAMPLE: USING STRAIN-SOFTENING TO DETERMINE THE EXTENT OF THE YIELD ZONE

Originally, this example was formulated using U.S. customary units of measurement. Conversion to the metric system makes some values appear awkward.

GROUP 1: 0-2 m INTO THE PILLAR

Input Parameters:

$S_1 = 3.5$ MPa
$F_{insitu} = 6.9$ MPa
Entry width (2a) = 6 m
a = 3 m
Extension of group 1 (e_1) = 2 m
h = 2 m
$a_{eff1} = a + e_1 = 5$ m

The first group of point forces simulates the post strength for group 1, which is the first 2 m into the pillar (figure 20). These point forces are uniform; therefore, it is necessary to use equation 19 to determine an average strength value. This value will be assigned the point forces in group 1. An estimate of the average point force for group 1 would be determined from equation 19 for a point 1 m into the pillar.

$$F_{avg} = F_v(1\,m) = 3.5\left(0.78 + 1.74\,\frac{1}{2}\right) = 5.8 \text{ MPa}$$

The stress intensity relating to this average point force is taken from equation 15 as

$$K_{ps_{1,1}} = \frac{F_{avg}}{\sqrt{Ba_{eff}}} \int_a^{a_{eff}} \left(\sqrt{\frac{a_{eff} + x}{a_{eff} - x}} + \sqrt{\frac{a_{eff} - x}{a_{eff} + x}} \right) dx .$$

Equation 16 solves this integral as

$$K_{ps_{1,1}} = 2F_{avg}\sqrt{\frac{a_{eff}}{B}}\cos^{-1}\frac{a}{a_{eff}}$$

$$K_{ps_{1,1}} = 2\left(5.8\sqrt{\frac{5}{B}}\cos^{-1}\frac{3}{5}\right.$$

$$= 13.6$$

$$K_{ps_{total}} = K_{ps_{1,1}}$$

$$= 13.6$$

The stress intensity for group 1 in absence of the point forces is

$$K_{a_{eff1}} = 6.9\sqrt{B(3+2)}$$

$$= 27.3$$

$K_{ps\ total}$ is less than K_{aeff1}; therefore, this section is yielded and the crack extends to the end of the next section (group 2). The coal continues to yield until the residual pillar stress overcomes the in situ Westergaard stress.

GROUP 2: 2-4 m INTO THE PILLAR

Input Parameters:

$e_2 = 2$ m
$a_{eff1} = 5$ m
$a_{eff2} = a_{eff1} + e_2 = 7$ m
Midpoint of group 2 is 3 m into the pillar

The crack tip is extended 4 m (i.e., $e_1 + e_2$) to the end of group 2. This makes a_{eff2}, the effective crack tip, equal to 7 m. Using equation 19, the average stress in this section is 11.9 MPa. This is the post strength determined for a location 3 m into the pillar. The stress intensity caused by the wedge forces in group 2 is

$$K_{ps_{2,2}} = 2\left(11.9\sqrt{\frac{7}{B}}\cos^{-1}\frac{5}{7}\right.$$

$$= 27.5$$

It is necessary to also consider the stress intensity caused by the residual point forces in group 1. Because the crack tip extended into the 2-to 4-m (group 2) section of the yield zone, it is necessary to recalculate the effect of the 0- to 2-m (group 1) section of the yield zone:

$$K_{ps_{1,2}} = \frac{5.8}{\sqrt{B7}}\int_3^5\left(\sqrt{\frac{7+x}{7-x}}+\sqrt{\frac{7-x}{7+x}}\right)dx$$

"Derive—A Mathematical Assistant" determined this value to be:

$$K_{ps_{1,2}} = 6.1$$

The total stress caused by the point forces is

$$K_{ps_{total}} = K_{ps_{2,2}} + K_{ps_{1,2}}$$

$$= 33.6$$

The stress intensity caused by the crack extension to the end of group 2 in absence of the residual point forces is

$$K_{a_{eff2}} = 6.9\sqrt{B(5+2)}$$

$$= 32.3$$

This stress factor is less than the stress intensity due to the residual strength point forces ($K_{aeff2} < K_{ps\ total}$); thus, the yielding ceases in group 2. Because the values are nearly equal, the crack extended almost to the end of group 2 (i.e., 4 m into the pillar). It is possible to refine this distance, but it is unnecessary for this example. Equation 19 will predict the stress distribution in the yield zone; the Westergaard equation will predict the distribution in the elastic core.

Irwin suggests a way to use the Westergaard equation to predict the stress distribution in the pillar's elastic core (at the edge of the yield zone) [Broek 1982]. Irwin agrees with Dugdale's prediction for the extent of the yield zone, but he argues that the crack tip extends into this zone one-half the distance predicted by Dugdale such that

$* = D/2 = 2$ m (in the previous example).

This increases the effective crack width to

$$a_{eff} = a + * = 5 \text{ m}.$$

This is the beginning of the Irwin zone—the region from which the Westergaard equation predicts the stress distribution into the core of the material (figure 21).

Extending the crack tip to the beginning of the Irwin zone, the Westergaard equation becomes

$$F_{Irwin\ zone} = \frac{F_{insitu}x}{\sqrt{x^2-(a+*)^2}}. \qquad (21)$$

Although the x-origin in the Westergaard equation begins in the Irwin zone, the stress distribution does not take effect until the beginning of the elastic zone. Equation 19 describes the stress distribution throughout the entire yield zone. Figure 22 shows the stress distribution for the combined strain-softening and analytic models.

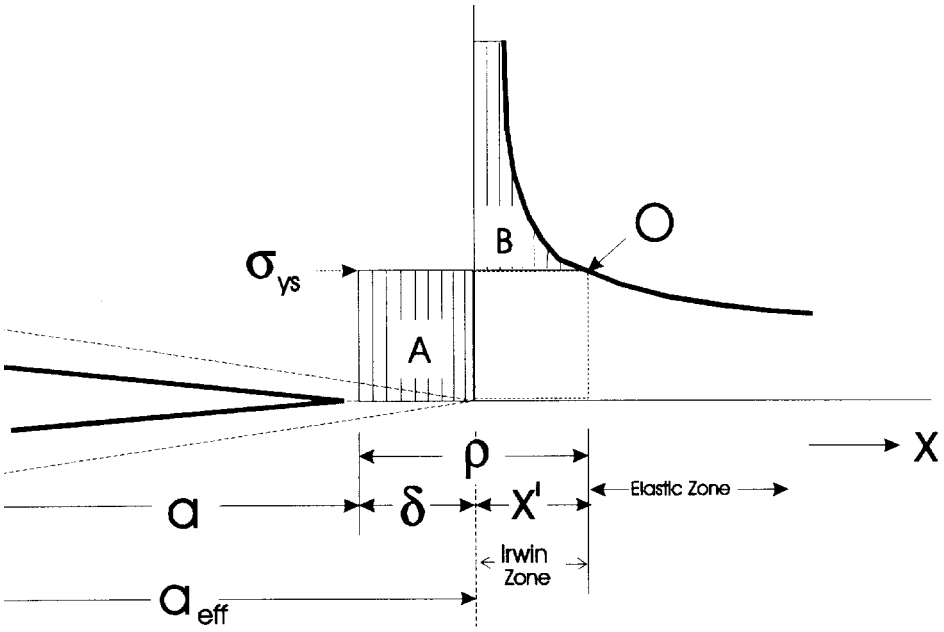

Figure 21.—The Westergaard equation begins in the Irwin zone; it takes effect in the elastic zone.

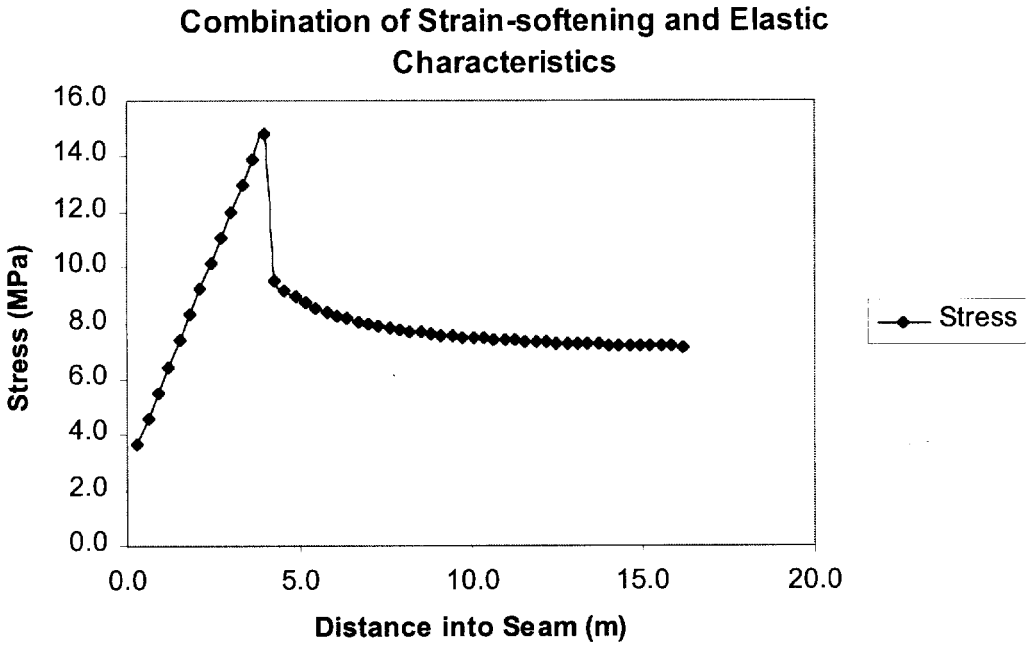

Figure 22.—Strain softening in the process zone and a Westergaard distribution in the elastic zone.

SUPERPOSITION

A mine opening affects the stress distribution at each of its sides. A mine panel is a gridwork of regularly or irregularly spaced entries and crosscuts.[9] For a complete stress analysis, it is necessary to consider the stress influences caused by every mine passageway. A superposition technique makes this possible [Kramer 1996].

The superposition technique requires subdividing the stress distribution into its constitutive components (figure 23). Each side of the pillar is subjected to a Westergaard stress distribution. Restricting the pillar model to two dimensions, as in the case of plane strain, limits these distributions to the left and right sides of the pillar. The basic components needed in the superposition are the uniform in situ stress, the stress component from the left opening, and the stress component from the right opening. The right and left stress components are each equal to the Westergaard equation with the in situ stress removed such that

$$F_{component} = \frac{F_{insitu} x}{\sqrt{x^2 - a^2}} - F_{insitu}. \qquad (22)$$

[9]An entry is a tunnel aligned in the main direction of mining. A crosscut connects individual entries, usually at a right angle. Several entries and crosscuts comprise a mine panel. A pillar is coal remaining in place between two entries and crosscuts; it supports the mine roof.

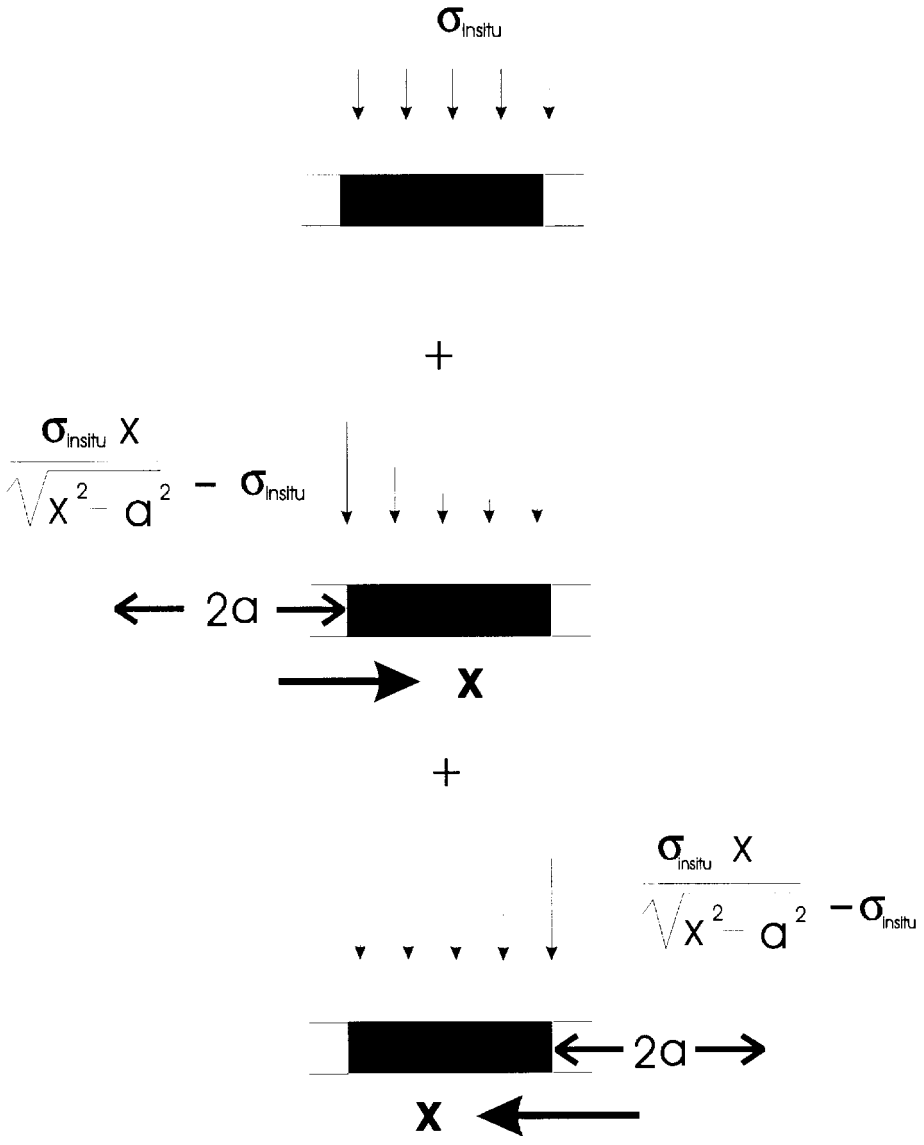

Figure 23.—Pillar stress broken down into three components.

The left stress component has the origin of its axis located to the left of the pillar. The positive direction, relative to this axis, is rightward from the origin into the pillar. The right component is the mirror image of the left. This component has the origin of its axis to the right of the pillar. The variable "a" can have a different value for each side of the pillar (figure 23). The total stress distribution on the pillar is equal to the left component plus the uniform in situ stress plus the right component. As verified by FLAC, the superposition technique accurately predicts the stress distribution across a single pillar (figure 24).

A mine opening affects the stress distribution for a substantial distance. A mine panel consists of a gridwork of entries and crosscuts. It is necessary to superimpose the stress components from all mine passageways. FLAC compares the results of the superposition across an entire mine panel (figure 25).

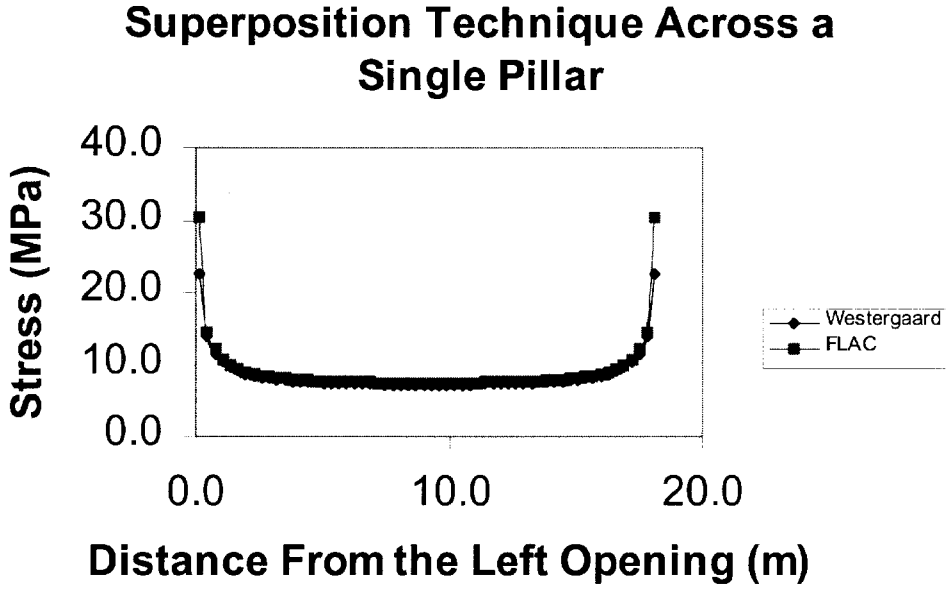

Figure 24.—Pillar with stress superimposed from both sides.

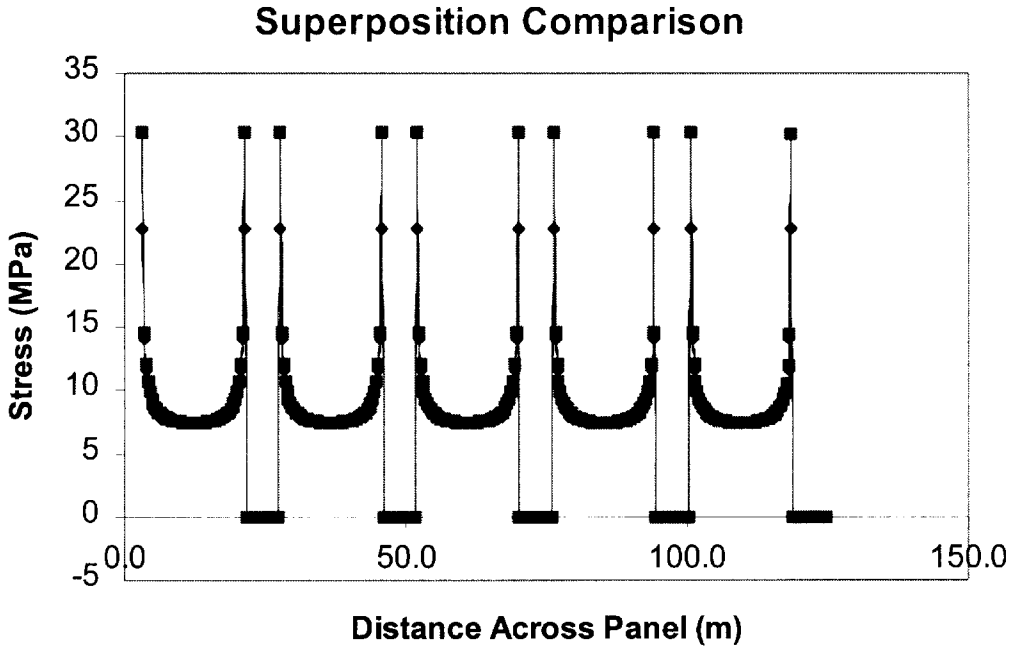

Figure 25.—Westergaard equation and superpositioning stress over an entire mine panel. Comparison with numerical model.

POSSIBLE ENHANCEMENTS

It is possible to enhance the modeling capabilities of the FMA. Adding other techniques would give the ability to analyze displacements in the strata, creep behavior in mine supports, and the effects of multiple-seam mining. Because the FMA is straightforward and easy to use, there is potential to model many different mining situations.

The following sections discuss some possible additions to the FMA. Although each technique presented seems reasonable, no comparison has been made with numerical analysis to qualify accuracy.

VIEW OF STRESS DISTRIBUTION FROM A PLANAR PERSPECTIVE

Sometimes it is desirable to study the stress distribution looking down on the coal seam (planar view) instead of into it (cross-sectional view). In a planar view, coal pillars are rectangular. The corners of the pillar generate mathematical singularities that create problems for analysis. One way to eliminate the singularities is to assume the pillar is an ovaloid instead of a rectangle [Kramer 1996]. It is possible to segment the pillar into concentric ovaloid lines of equal distance (figure 26). Fracture mechanics predicts the stress distribution through the pillar centers, as indicated by the vertical and horizontal lines in figure 26. An interpolation technique can approximate the stress throughout the pillar by using the concentric ovaloid arcs as interpolation pathways. For instance, the arc segment between points A and B in figure 26 would be the interpolation path between the stresses at points A and B. It is easy to interpolate the stresses along ovaloid paths. The basic equations for mapping elliptical coordinates to Cartesian coordinates are:

$$x = a \cos 2 \qquad y = b \sin 2 \qquad (23)$$

An example of the interpolation process follows.

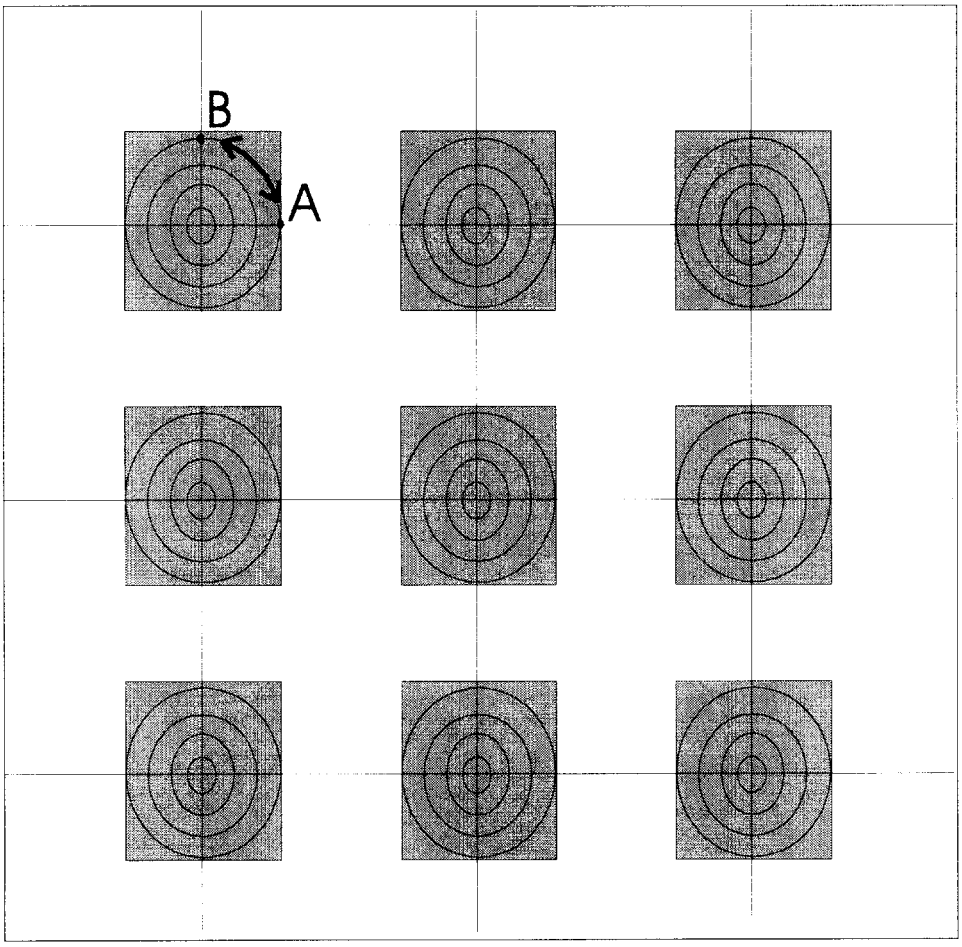

Figure 26.—Fracture mechanics predicts the center stress in both directions through the pillar. An interpolation technique translates the stress along the elliptical trajectories.

EXAMPLE OF INTERPOLATION

Considering the elliptical path shown in quadrant I of figure 27, interpolate the stresses along path A-B in the outer arc of quadrant I. For this example, assign the following properties:

$F_A = 1{,}000$ psi

$F_B = 1{,}500$ psi

$a = 20$

$b = 10$

Divide 2 into five equal angles:

$$\frac{90}{5} = 18° \tag{24}$$

Determine the stress interpolation interval for each 18° arc:

$$\frac{1{,}500 \text{ psi} - 1{,}000 \text{ psi}}{5 \text{ intervals}} = 100 \text{ psi per interval} \tag{25}$$

Figure 28 illustrates the stress distribution along this arc. Equation 24 relates any point on the A and B axis to any point on the ovaloid (figure 27). Therefore, it is possible to approximate the stress distribution throughout the entire pillar.

VISCOELASTICITY

Sih [1966] and Paris and Sih [1965] discuss crack behavior in viscoelastic (time-dependent) material. For viscoelastic material, the crack-tip stress field is the same, only the stress intensity factors K_I are functions of time, such that

$$K_I = K_I(t) \tag{26}$$

This function shows promise for future applications using the FMA. For instance, it could be valuable for studying the behavior of salt.

DISPLACEMENTS

Fracture mechanics may also predict the displacement/strain in a mine environment. A common method to predict displacement is referred to as the "crack opening displacement" (COD) [Broek 1982]. The COD method takes into account the total displacement of the crack surface (figure 29). In mining, the COD predicts the combined displacement of the roof and floor of an opening, such that

$$\text{COD} = 2v = \frac{4F}{E}\sqrt{a^2 - x^2} \tag{27}$$

and at the center of the opening:

$$\text{COD}_{max} = 2v = \frac{4Fa}{E}. \tag{28}$$

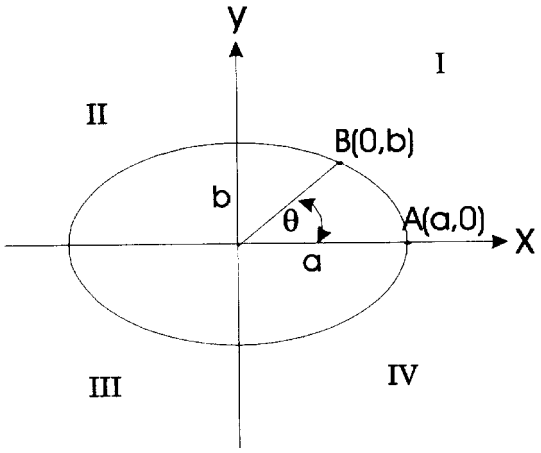

Figure 27.—Relationship between elliptical and rectilinear coordinates.

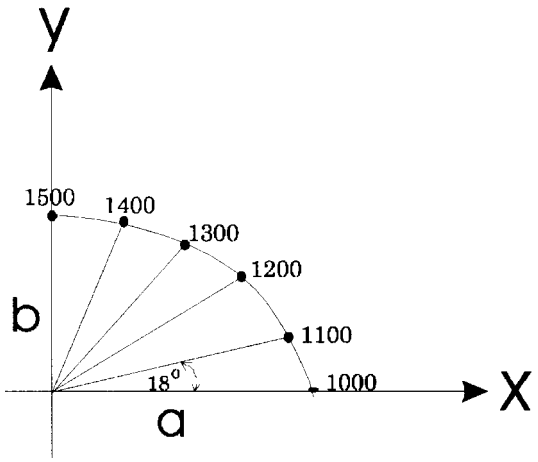

Figure 28.—Stresses distributed along interpolation arc.

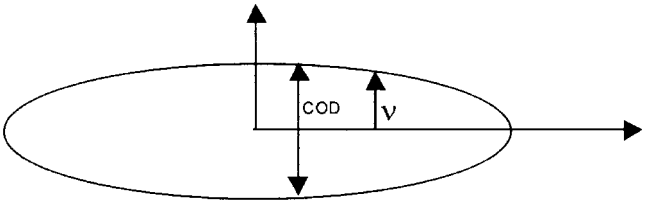

Figure 29.—The crack opening displacement (COD) method considers the displacement of the entire surface of a crack.

MULTIPLE-SEAM MINING

It may be possible to predict the effects on stress distribution caused by mining activity in seams above or below the area of interest. By using stress influence functions developed for mine subsidence prediction, it should be possible to predict multiple-seam influences with a respectable degree of accuracy [Luo 1997]. This multiple-seam model could be more accurate than other numerical methods because most other methods use influence functions based on the theory of elasticity, which assumes infinitesimal displacements. Using influence functions based on mine subsidence profiles takes into account the well-documented, large-scale displacements measured at various mine locations.

CONCLUSION

This paper presents the FMA for predicting the stresses in a mine panel. It can model any combination of mine supports such as longwall gob, yield pillars, cribs, chocks, posts, automated temporary roof supports, and hydrostatic loads. The technique uses an analytic expression; thus, it is fast, simple, and accurate. It simulates pillar yield by combining the analytic equation with any empirical pillar strength equations. The procedure incorporates easily into spreadsheets or computer software. The FMA predicts pillar stress with a high degree of accuracy; however, it is no match to good numerical modeling software. Its main function is to be quick and simple in order to encourage nonspecialized personnel to use it as a guide for studying mine supports.

The FMA works well for coal seams aligned along a horizontal plane. Additional effort is needed to assess its accuracy for seams aligning along inclined planes. More work is also necessary to develop FMA techniques for thick-seam mining, multiple-seam mining, and displacement prediction. Computer software featuring the FMA is available from the author.

REFERENCES

Barenblatt G [1962]. The mathematical theory of equilibrium of cracks in brittle fracture. Advances in Appl Mech *7*:55-129.

Berry D [1960]. An elastic treatment of ground movement due to mining isotropic ground. J Mech Phys Solids *8*:280-292.

Berry D [1963]. Ground movement considered as an elastic phenomenon. Trans Inst Min Eng *123*:28-41.

Broek D [1982]. Elementary engineering fracture mechanics. 3rd ed. The Hague, The Netherlands: Martinus Mijhoff Publishers.

Crouch SL, Fairhurst C [1973]. The mechanics of coal mine bumps and the interaction between coal pillars, mine roof, and floor. U.S. Department of the Interior, Bureau of Mines, OFR 53-73.

Dugdale D [1960]. Yielding of steel sheets containing slits. J Mech Phys *8*:100-108.

Hacket P [1959]. Analytic analysis of rock movements caused by mining. Trans Inst Min Eng *118*(7):421-433.

Karabin GJ, Evanto MA [1999]. Experience with the boundary-element method of numerical modeling to resolve complex ground control problems. In: Proceedings of the Second International Workshop on Coal Pillar Mechanics and Design. Pittsburgh, PA: U.S. Department of Health and Human Services, Public Health Service, Centers for Disease Control and Prevention, National Institute for Occupational Safety and Health, DHHS (NIOSH) Publication No. 99-114, IC 9448.

Kramer JM [1996]. The use of fracture mechanics to predict the stress distribution in coal mine pillars [Dissertation]. Morgantown, WV: West Virginia University, Department of Mining Engineering.

Kramer JM, Luo Y, Peng SS [1998]. An analytic approach to determine the stress distribution in longwall chain pillars. In: Peng SS, ed. Proceedings of the 17th International Conference on Ground Control in Mining. Morgantown, WV: University of West Virginia, pp. 162-168.

Luo Y [1997]. Private conversation between J. Kramer, Mine Safety and Health Administration, and Y. Luo, West Virginia University, Morgantown, WV.

Mark C, Iannacchione AT [1992]. Coal pillar mechanics: theoretical models and field measurements compared. In: Proceedings of the Workshop on Coal Pillar Mechanics and Design. Pittsburgh, PA: U.S. Department of the Interior, Bureau of Mines, IC 9315, pp. 78-93.

Paris P, Sih G [1965]. Stress analysis of cracks. ASTM STP *391*: 30-81.

Salamon MDG, Munro AH [1967]. A study of the strength of coal pillars. J S Afr Inst Min Metall *68*:55-67.

Sih G [1966]. On the Westergaard method of crack analysis. Inter J Fracture Mech *2*:628-631.

Westergaard H [1939]. Bearing pressures and cracks. ASME J of Appl Mech *61*:A49-53.

Wilson AH [1972]. An hypothesis concerning pillar stability. Min Eng (London) *131*(141):409-417.